Elasticity theory for self-assembled protein lattices with application to the martensitic phase transition in bacteriophage T4 tail sheath

Wayne Falk*
Department of Diagnostic and Biological Sciences, University of Minnesota, Minneapolis, Minnesota 55455, USA

Richard D. James†
Department of Aerospace Engineering and Mechanics, University of Minnesota, Minneapolis, Minnesota 55455, USA

(Received 17 August 2005; revised manuscript received 23 November 2005; published 27 January 2006)

We propose an elasticity theory for one- and two-dimensional arrays of globular proteins for which the free energy is affected by relative position and relative rotation between neighboring molecules. The kinematics of such assemblies is described, the conditions of compatibility are found, a form of the free energy is given, and formulas for applied forces and moments are developed. It is shown that fully relaxed states of sheets consist of helically deformed sheets which themselves are composed of helical chains of molecules in rational directions. We apply the theory to the fascinating contractile deformation that occurs in the tail sheath of the virus bacteriophage T4, which aids its invasion of its bacterial host. Using electron density maps of extended and contracted sheaths, we approximate the domains of each molecule by ellipsoids and then evaluate our formulas for the position and orientation of each molecule. We show that, with the resulting kinematic description, the configurations of extended and contracted tail sheaths are generated by a simple formula. We proposed a constrained version of the theory based on measurements on extended and contracted sheath. Following a suggestion of Pauling [Discuss. Faraday Soc. **13**, 170 (1953)], we develop a simple model of the molecular interaction. The resulting free energy is found to have a double-well structure. Certain simple deformations are studied (tension, torsion inflation); the theory predicts a first-order Poynting effect and some unexpected relations among moduli. Finally, the force of penetration is given, and a possibly interesting program of epitaxial growth and patterning of such sheets is suggested.

DOI: 10.1103/PhysRevE.73.011917 PACS number(s): 87.10.+e

I. INTRODUCTION

A remarkably large number of biological structures are composed of identical protein molecules, or mixtures of a few different protein molecules, in regular arrays. Examples are microtubules, bacterial flagella, F-actin filaments, and viral coats. These are different from typical inorganic crystals in that the individual molecules are composed of many atoms and the whole array is typically not a three-dimensional (3D) crystal but is often a single-molecule-thick regular array on a sheet, either flat, curved, or polyhedral, or else in a linear chain. Often the latter adopt helical forms, and, in the example below of the bacteriophage T4 tail sheath, the cylindrical sheath is composed of two families of helical chains of proteins. Besides the reduced dimensionality and natural curvature, the protein-protein interactions involve one or more bonding sites with groups of bonded atoms distributed over the bonding site. Because of this, the interactions can be complex (from a first principles' viewpoint) and proteins exert both forces and moments on each other. However, a simplifying feature of the interactions is that individual protein molecules in such arrays predominantly interact only with nearest neighbors.

With the rapid development of optical tweezers and atomic force microscopes [1,2], it has become possible to subject a protein structure to a force or moment and to measure its elastic response. These experiments seem to be often interpreted in terms of classical macroscopic theories of elasticity. For example, Kirchhoff's rod theory is often used to interpret experiments on chains such as DNA [3–5]. As discussed by these authors, Kirchhoff's rod theory is expected to be valid when the length of the chain is much larger than its diameter and helical pitch, and it has been used successfully in such cases. But Kirchhoff's rod theory is built on certain assumptions relating to the macroscopic theory of nonlinear elasticity. Thus, for example, in its simplest anisotropic form, three suitable bending-torsion experiments suffice to determine the moduli, meaning that the mechanical behavior in all subsequent experiments is then determined. In addition, with only a few molecules (138 in the case of the T4 tail sheath) or with localized large curvatures, a molecular elasticity theory may be needed.

For these reasons we develop here an elasticity theory that is suitable for these protein arrays. The proteins themselves have irregular yet well-defined shapes and they interact via localized bonding sites. We steer a course midway between detailed first principles calculations on the given protein sequence (which, at present, would leave us stuck on the protein folding problem) and macroscopic nonlinear elasticity. First, each molecule is given a position and orientation. We explain how position and orientation are related to detailed structure, in a manner that is consistent with the results of first principles calculations. Our definition is different from the usual one, but seems to have some advantages. It also has

*Electronic address: falk@aem.umn.edu
†Electronic address: james@umn.edu

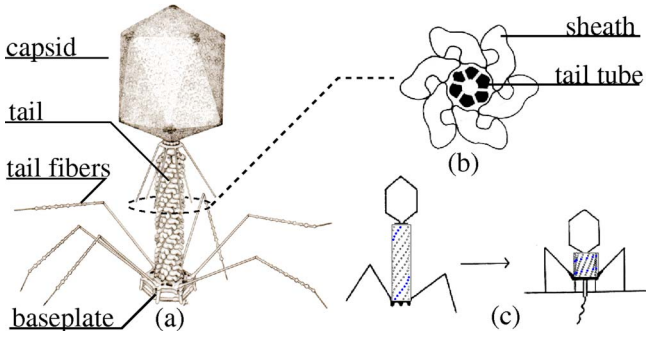

FIG. 1. (Color online) (a) Structure of bacteriophage T4, based on electron microscope structure analysis to a resolution of about 2–3 nm, from [6]. Reproduced with permission of Fred Eiserling. (b) A cross section showing concentric tail tube and sheath annuli. (c) Schematic of contraction process [7].

the property that the position and orientation are given by a translation and rigid rotation of a reference molecule that best approximates, in a least squares sense, the deformed molecule. As for interactions, we focus on pairwise forces and moments, because bonding between globular proteins is often localized at the region of contact between two proteins. Because we have an orientation variable as well as a positional one, our theory also has points of contact with the theory of liquid crystals, but in the end the theory is quite different.

We propose a form of the free energy based on these ideas (Sec. III). Imposing the condition of frame indifference, we define certain "strain variables" upon which the free energy depends. Conditions of compatibility concern the extent to which these strain variables can be assigned independently: for sheets, we find that necessary and sufficient conditions for compatibility (of a simply connected sheet, defined precisely below) are that a certain pair of sums of four terms vanishes. These relate to the process of checking compatibility around elementary squares consisting of four molecules. We find these conditions to be very useful.

For both chains and sheets, helical configurations arise as the natural ordered structures. In particular, under general conditions they are the free energy minimizers in the absence of boundary conditions. These results can be considered as analytical expressions of the ideas of Crane [8]. Ultimately the reason is the same reason that these configurations are natural in nonlinear elasticity (Ericksen [9]). To oversimplify, in a helical configuration any two parts of the chain, of equal monomer length, are related by a Euclidean transformation. Therefore, the equilibrium of a short section implies, via rotation and translation, that the whole helix is in equilibrium. In the present context they play a deeper role: fully relaxed states of a sheet governed by our free energy consist of helically deformed sheets which themselves are composed of helical chains of molecules (Sec. VIII).

Using this theory, we study of deformations of the tail sheath of bacteriophage T4 (Fig. 1). Bacteriophages are viruses that attack bacteria. The T4 virus is composed of a *capsid* containing the viral DNA [Fig. 1(a)] and a *tail* shown extending down from the capsid. The tail consists of a pair of concentric cylinders [Fig. 1(b)] each about 1000 Å long. The inner *tail tube* with a diameter of about 90 Å is surrounded by the tail sheath with an outer diameter of about 240 Å. The sheath is composed of six parallel helices, made from chains of a single type of protein. Although the tail sheath is a single molecular layer protein sheet, it should not be considered (as is assumed by nonlinear plate theory) thin relative to its radius of curvature, this ratio being (thickness)/(mean radius of curvature) ≈ 1.

Prior to invasion of the host, the sheath proteins are arranged as steeply pitched helices, and the tail adopts so-called *extended* structure. During the virus' attack on a bacterium, the tail sheath changes shape dramatically; the protein helices compress, causing the sheath to shorten and fatten into a more compact *contracted* structure. This drives the relatively rigid inner tail tube through the cell wall, making a passage for the viral DNA to pass into the host [Fig. 1(c)]. During this process the sheath contracts irreversibly to about 1/3 of its original length accompanied by a 50% increase in outer diameter. The transformation has many features in common with martensitic phase transformations, as has been noted by Olson and Hartman [7]. For a general review of T4 tail structure and function see Rossmann *et al.* [10].

Once the viral DNA is inside the host, it reprograms the host cell to produce all ingredients needed to form new viruses. The viral protein molecules produced by this process self-assemble into virus progeny within the host, eventually causing it to burst, releasing the viruses to infect other hosts.

We apply the theory of the protein sheet to the tail sheath of bacteriophage T4. Using measured electron density maps of extended and contracted sheath [11,12], we identify three domains in each molecule and approximate these by ellipsoids. We then define the structures of the two phases. We develop a simple formula that produces these structures [Eq. (40)], and applies to any any model of the molecule, however complex. The simplicity of this formula arises from the fact that, even though the molecule itself may be complex, the relationship between different molecules is very simple. Based on the experimentally observed mode of deformation, we adopt a constrained theory for the sheath. The constraints are exactly satisfied by both extended and contracted sheath. The resulting theory has surprising implications with regard to the response of the sheath to different loadings, including a strong first order Poynting effect, unexpected relations between moduli, certain combinations of applied axial force and moment that do no work on the sheath, and a certain relation between the force and moment needed to transform contracted to extended sheath. Among these results, there are numerous possible points of comparison with future small-scale quantitative experiments.

A very early model of helical contraction proposed by Pauling [13] provides a basis for simplifying our free energy. Pauling envisioned that helices forming a cylinder could be compressed to the point where adjacent turns of the helix would form bonds. This leads to a simple model of interactions with one family of bonds guiding assembly and another causing contraction. As higher resolution images of the T4 tail sheath become available [11], this remains likely the principal mechanism for sheath contraction. Guided by Pauling's mechanism, we build a simplified free energy for the T4 tail sheath.

The deformation of the T4 tail sheath is a particularly interesting case for the theory for several reasons: (1) very large changes of shape in an organized protein structure take place as a means of producing force, (2) the shape change has been identified as of martensitic type, which suggests a multiwell elasticity theory, and (3) there is an interest in understanding how this phase transformation relates to nonbiological martensitic transformations, and in particular how the force and energy of contraction compare in the biological and nonbiological cases. The latter could suggest strategies for manmade analogs of the T4 tail sheath. Finally, (4) a quantitative evaluation of the energy stored has interesting biological significance. That is, in bacteriophage T4, as in all viruses, there is no mechanism for the production of energy. Thus, all the energy that is released upon contraction of the tail sheath must be stored during the assembly phase of the virus, from apparently high free energy molecules created during translation of the viral genome, aided by the energy consuming translation mechanism of the bacterial host. For the purpose of storage of this energy, the process of epitaxial stabilization, familiar from the growth of semiconductor compounds on single crystal substrates, apparently plays an important role. Motivated by these ideas we suggest such a program of epitaxy (Sec. X).

Mathematical notation. Boldfaced uppercase letters are 3×3 matrices and boldfaced lowercase letters are vectors in $\mathbb{R}^3$. Components are relative to a fixed orthonormal basis throughout. Lowercase greek letters denote components of vectors while lowercase latin letters are indices for molecules, e.g., the (i,j)th molecule of a sheet. $\mathbb{Z}^2$ denotes all pairs of integers (i,j). The summation convention is used; $\mathbf{A}\cdot\mathbf{B}$ is the inner product between matrices, $\mathbf{A}\cdot\mathbf{B}=A_{\alpha\beta}B_{\alpha\beta}$, and $\|\mathbf{A}\|=\sqrt{\mathbf{A}^T\mathbf{A}}$. The superscript T denotes transpose, $\mathrm{tr}\mathbf{A}=A_{\alpha\alpha}$ is the trace of $\mathbf{A}$, $\mathbf{I}$ is the identity matrix, $(\mathbf{a}\otimes\mathbf{b})$ is the matrix with components $a_\alpha b_\beta$, $\mathrm{Skew}\mathbf{A}=(1/2)(\mathbf{A}-\mathbf{A}^T)$, and 3×3 rotation matrices are denoted by $\mathrm{SO}(3)=\{\mathbf{R}:\mathbf{R}^T\mathbf{R}=\mathbf{I},\det\mathbf{R}=+1\}$.

II. KINEMATIC DESCRIPTION OF INDIVIDUAL PROTEIN MOLECULES, CHAINS, AND SHEETS

We are interested in chains and sheets consisting of protein molecules. For simplicity we shall consider both structures to consist of identical molecules.[1]

A molecule will be specified by a pair $(\mathbf{y},\mathbf{R})$ consisting of a position vector $\mathbf{y}\in\mathbb{R}^3$ and a rotation matrix $\mathbf{R}\in\mathrm{SO}(3)$, termed, respectively, position and orientation. Protein chains and sheets are constructed by building up one- and two-dimensional arrays of these molecules. For chains we choose a set of integers $\{1,\ldots,N\}$ corresponding to N molecules and assign mappings

$$\mathbf{y}:\{1,\ldots,N\}\to\mathbb{R}^3,\quad \mathbf{R}:\{1,\ldots,N\}\to\mathrm{SO}(3). \tag{1}$$

For sheets we denote molecules by pairs of integers $(i,j)\in\mathbb{Z}^2$. We consider a set $\mathcal{D}=\{1,\ldots,N\}\times\{1,\ldots,M\}$ and mappings

$$\mathbf{y}:\mathcal{D}\to\mathbb{R}^3,\quad \mathbf{R}:\mathcal{D}\to\mathrm{SO}(3). \tag{2}$$

For the configuration of a single molecule we use the obvious notation $(\mathbf{y}_i,\mathbf{R}_i)$ for chains and $(\mathbf{y}_{i,j},\mathbf{R}_{i,j})$ for sheets. More generally, $\mathcal{D}$ could have the form $\Omega\times\mathbb{Z}^2$ where Ω is a domain in the plane.

The usual way to define orientation of a molecule, or a collection of molecules, is to take moments of the (time averaged) mass distribution (see, e.g., de Gennes [14], Chap. 2), typically the second or fourth moment. Below, we suggest a different definition of orientation that seems to have advantages with regard to the connection with molecular dynamics simulation.

Each molecule consists of ν atoms of C, H, and various other elements in a folded configuration. For each atom we assign a corresponding atomic mass m_i, $i=1,\ldots,\nu$. Near physiological temperatures, the atoms in a protein molecule undergo rather large vibrations, but it is still sensible to talk about the time averaged position on macroscopic time scales and we shall assign these average positions as $\mathbf{y}_1,\ldots,\mathbf{y}_\nu$. Time averaged momentum has dynamical significance, so we use it to define the position of a molecule. We will take its *position* to be its mass averaged position,

$$\mathbf{y}=\frac{\sum_{i=1}^{\nu} m_i\mathbf{y}_i}{\sum_{i=1}^{\nu} m_i}. \tag{3}$$

From the same information we can also obtain a measure of the orientation of a molecule. That is, we consider a molecule in standard position defined by fixed atomic positions $\mathbf{x}_1,\ldots,\mathbf{x}_\nu$. This standard position could for example be the collection of positions in a crystallized form of the molecule, deduced from x-ray crystallography, or from theoretical studies of the configuration of single molecules in solution. From these reference positions we define the mass averaged reference position as above,

$$\mathbf{x}=\frac{\sum_{i=1}^{\nu} m_i\mathbf{x}_i}{\sum_{i=1}^{\nu} m_i}. \tag{4}$$

A natural concept of orientation is obtained through the average deformation gradient of the molecule, defined in the following way:

$$\mathbf{F}=\frac{\sum_{i=1}^{\nu} m_i(\mathbf{y}_i-\mathbf{y})\otimes(\mathbf{x}_i-\mathbf{x})}{r^2\sum_{i=1}^{\nu} m_i}. \tag{5}$$

Here, r can be taken as a typical radius of the reference molecule, e.g.,

[1]The extension to regular arrays of several different proteins is expected to be similar.

$$r = \sqrt{\frac{\sum m_i(\mathbf{x}_i - \mathbf{x})^2}{\sum m_i}}. \tag{6}$$

(The position and orientation of a molecule will turn out to be independent of r.) The expression (5) for $\mathbf{F}$ is dimensionless and translation invariant. Typically, it will be true that $\det \mathbf{F} > 0$, which we assume. If the $\mathbf{y}_i$ represent a rigid deformation of the reference molecule, i.e., $\mathbf{y}_i = \mathbf{Q}\mathbf{x}_i + \mathbf{c}$, $i = \{1, \ldots, \nu\}$, $\mathbf{Q} \in \mathrm{SO}(3)$, then it follows from Eq. (5) that

$$\mathbf{F} = \mathbf{Q}\mathbf{V}, \tag{7}$$

where

$$\mathbf{V} = \frac{\sum_{i=1}^{\nu} m_i(\mathbf{x}_i - \mathbf{x}) \otimes (\mathbf{x}_i - \mathbf{x})}{r^2 \sum_{i=1}^{\nu} m_i}. \tag{8}$$

The latter is interpretable as a normalized reference moment of inertia. In general we will use the rotation in the polar decomposition of $\mathbf{F}$ as a measure of orientation. That is, we will write

$$\mathbf{F} = \mathbf{R}\mathbf{U} \text{ where } \mathbf{R} \in \mathrm{SO}(3) \text{ and } \mathbf{U} = \mathbf{U}^T \text{ is positive definite}, \tag{9}$$

and define $\mathbf{R}$ in this decomposition as the *orientation*. For molecules that deform as well as rotate and translate, $\mathbf{R}$ is still a natural measure of orientation.

These definitions of position and orientation, the latter defined by a polar decomposition of the apparently complicated formula for $\mathbf{F}$, have several attractive features. First, we observe that both $\mathbf{F}$ and $\mathbf{y}$ are linear functions of the positions $\mathbf{y}_1, \ldots, \mathbf{y}_\nu$. We have framed the definitions in this way so that their second time derivatives are immediately related to (time averaged) forces via the equations of molecular dynamics. Second, there is a useful variational characterization of $\mathbf{R}$ and $\mathbf{y}$. That is, $\mathbf{R}(\mathbf{x}_i - \mathbf{x}) + \mathbf{y}$ is the rigid deformation that best approximates the mass distribution of the molecule in the least squares sense. More precisely, if we consider the rotation matrix $\mathbf{Q}$ and vector $\mathbf{c}$ that minimize[2]

$$\min_{\mathbf{c}, \mathbf{Q} \in \mathrm{SO}(3)} \int |\mathbf{y}(\mathbf{z}) - [\,\mathbf{Q}(\mathbf{z} - \mathbf{x}) + \mathbf{c})]|^2 dm(\mathbf{z}), \tag{10}$$

where dm is the mass measure of the molecule, i.e., $m = \Sigma m_i \delta_{x_i}$, and $\mathbf{y}(\mathbf{x}_i) = \mathbf{y}_i$, then it follows from the simple quadratic minimization problem (10) that $\mathbf{Q} = \mathbf{R}$ and $\mathbf{c} = \mathbf{y}$ as defined by Eqs. (3), (5), and (9). The proof of this fact is straightforward. First, by differentiating Eq. (10) with respect to $\mathbf{c}$ we conclude immediately that $\mathbf{c} = \mathbf{y}$. Then we replace $\mathbf{c} = \mathbf{y}$ in Eq. (10) and simplify. The minimization over $\mathbf{Q} \in \mathrm{SO}(3)$ then becomes

$$\begin{aligned} \min_{\mathbf{Q} \in \mathrm{SO}(3)} [-\mathrm{tr}(\mathbf{Q}^T\mathbf{F})] &= -\max_{\mathbf{Q} \in \mathrm{SO}(3)} \mathrm{tr}(\mathbf{Q}^T\mathbf{F}) \\ &= -\max_{\mathbf{Q} \in \mathrm{SO}(3)} \mathrm{tr}(\mathbf{Q}^T\mathbf{R}\mathbf{U}) = -\max_{\bar{\mathbf{Q}} \in \mathrm{SO}(3)} \mathrm{tr}(\bar{\mathbf{Q}}\mathbf{U}) \\ &= -\max_{\bar{\mathbf{Q}} \in \mathrm{SO}(3)} \sum_{\alpha} \lambda_\alpha \mathbf{e}_\alpha \cdot \bar{\mathbf{Q}}\mathbf{e}_\alpha, \end{aligned} \tag{11}$$

where $\{\mathbf{e}_1, \mathbf{e}_2, \mathbf{e}_3\}$ are orthonormal eigenvectors of $\mathbf{U}$ with corresponding positive eigenvalues $\{\lambda_1, \lambda_2, \lambda_3\}$. It is immediately seen that the latter maximization problem is uniquely solved by $\bar{\mathbf{Q}} = \mathbf{I}$, implying that $\mathbf{Q} = \mathbf{R}$.

The orientation $\mathbf{R}$ can be obtained from the formula $\mathbf{R} = \mathbf{F}\mathbf{U}^{-1} = \mathbf{F}(\sqrt{\mathbf{F}^T\mathbf{F}})^{-1}$, the square root being the unique positive-definite square root. For the purpose of a constrained molecular dynamic simulation (with given $\mathbf{R}$) it is useful to have a linear constraint. A necessary[3] condition that $\mathbf{R}$ is related to $\mathbf{F}$ by Eq. (9) is that $\mathrm{Skew}(\mathbf{R}\mathbf{F}^T) = 0$, that is,

$$\mathrm{Skew}\left[\mathbf{R}\left(\sum_{i=1}^{\nu} m_i(\mathbf{x}_i - \mathbf{x}) \otimes (\mathbf{y}_i - \mathbf{y})\right)\right] = 0, \tag{12}$$

which is a linear constraint on the $\mathbf{y}_i$.

In summary, our basic kinematics of a molecule is specified by a pair $(\mathbf{y}, \mathbf{R})$ defined by Eqs. (3), (5), (8), and (9). We wish to emphasize again that this choice of kinematics does not entail assumptions of rigidity of molecules. These formulas do allow one to determine our kinematic variables from unrestricted first principles calculations. We note that there are more complicated theories possible with this general type of kinematics. A further possible generalization would be that the free energy is affected by position and and full deformation gradient of molecules defined by (5).

III. FREE ENERGY

Although all atoms have infinite range, each protein molecule interacts primarily with its close neighbors and we shall develop the theory on this basis. Because bonding sites are often localized and interlocking, molecules are expected to exert both forces and moments on neighboring molecules.

We base the theory on a formula for the free energy. We make two simplifying assumptions which easily could be generalized: (1) the molecules are identical (thus we can use the reference configuration introduced in Sec. II for all molecules), and (2) we consider only nearest neighbor interactions. For chains, the "nearest neighbor" of $i \in \{2, \ldots, N-1\}$ refers to the two molecules $i-1, i+1$ for interior molecules while it refers to the molecule 2 for $i=1$ and $N-1$ for $i=N$. For sheets there are various possibilities. One can have triangular lattices with each molecule bonded to six nearest neighbors or rectangular lattices with each molecule having

[2] We write this as an integral rather than a sum to indicate that this characterization of $\mathbf{R}$ and $\mathbf{y}$ applies to any mass distribution.

[3] This condition is nearly sufficient for the determination of $\mathbf{R}$, the only freedom being that if $\mathbf{R}$ satisfies Eq. (12) then so does $\mathbf{R}\hat{\mathbf{R}}$ where $\hat{\mathbf{R}}$ is a 180° rotation about one of the eigenvectors of $\mathbf{U}$. In practice, if the configuration is changing slowly, this nonuniqueness would not cause a problem.

four nearest neighbors or more complicated situations. In the case of four nearest neighbors the nearest neighbors of (i,j) consist of all molecules of the form $(i+1,j),(i-1,j),(i,j+1),(i,j-1)$ that lie in $\mathcal{D}$. If not all four of these are in $\mathcal{D}$ we call (i,j) a *boundary molecule*; otherwise, we call it an *interior molecule*. Here we write the free energy only in the case of four nearest neighbors, the generalizations being automatic.

Since such protein arrays are of interest in solution, the assumptions are somewhat different than would be appropriate for atoms in a polymeric chain or a crystal. In particular the "free energy" will be taken as the free energy of the protein assembly and a fixed volume V of the surrounding solution. This is appropriate to the case that V is surrounded by a large bath B having fixed temperature and fixed chemical potentials of species in solution. All free energies below will depend on the temperature and chemical potentials, but since these will be fixed throughout this paper, we will leave these parameters out of the notation. As is well known the presence of the solution profoundly affects the free energy of the protein through osmotic effects, but it also affects the form of the free energy. In particular, boundary molecules may have a free energy that is different from interior molecules, because one or more of their bonding sites is unbonded and exposed directly to the solution.

In this simplest situation we will assume that, for chains, there is a molecular interaction free energy which depends on the position and orientation of a pair of molecules $\psi(\mathbf{a},\mathbf{R},\mathbf{b},\mathbf{Q})$ defined for $\mathbf{a},\mathbf{b}\in\mathbb{R}^3$ and $\mathbf{R},\mathbf{Q}\in \mathrm{SO}(3)$. In order to accommodate the possibility of boundary effects, we distinguish the free energy contribution from the interaction of the first and second molecules, $\psi_1(\mathbf{a},\mathbf{R},\mathbf{b},\mathbf{Q})$ and the next to last and last ones, $\psi_N(\mathbf{a},\mathbf{R},\mathbf{b},\mathbf{Q})$. The total free energy is then

$$\Psi(\mathbf{y}_1,\mathbf{R}_1,\ldots,\mathbf{y}_N,\mathbf{R}_N)=\sum_{i=2}^{N-2}\psi(\mathbf{y}_i,\mathbf{R}_i,\mathbf{y}_{i+1},\mathbf{R}_{i+1}) + \psi_1(\mathbf{y}_1,\mathbf{R}_1,\mathbf{y}_2,\mathbf{R}_2) + \psi_N(\mathbf{y}_{N-1},\mathbf{R}_{N-1},\mathbf{y}_N,\mathbf{R}_N). \quad (13)$$

The main physical assumption embodied here is that the contribution to the free energy from a pair of molecules is unaffected by the positions and orientations of all other molecules in the chain, in keeping with the idea that the main free energy changes are due to changes in conformation at the bonding site between a pair of molecules.

For sheets the assumptions are analogous. In this case there are 15 different kinds of boundary molecules, depending on which of the four bonds is missing. To simplify the notation we let $\mathcal{B}$ be the set of boundary molecules and write the total free energy as

$$\Psi(\mathbf{y}_{1,1},\mathbf{R}_{1,1},\ldots,\mathbf{y}_{N,M},\mathbf{R}_{N,M}) = \sum_{(i,j)\in\mathbb{Z}^2\cap\mathcal{D}\setminus\mathcal{B}}\psi_1(\mathbf{y}_{i,j},\mathbf{R}_{i,j},\mathbf{y}_{i+1,j},\mathbf{R}_{i+1,j}) + \psi_2(\mathbf{y}_{i,j},\mathbf{R}_{i,j},\mathbf{y}_{i,j+1},\mathbf{R}_{i,j+1}) + \sum_{(i,j)\in\mathcal{B}}\psi_{i,j}^{\mathcal{B}}, \quad (14)$$

where $\psi_{i,j}^{\mathcal{B}}$ is a free energy for the boundary molecules. Each $\psi_{i,j}^{\mathcal{B}}$ is one of the 15 functions describing the free energy of interaction of boundary molecules with dependence on the position and orientation of neighbors that are present. In writing this free energy, we have effectively assumed that all bonding sites of between molecules i,j and $i,j+1$ are the same, independent of i and j, and the same for sites of the form i,j and $i+1,j$. Also, in many interesting cases not all of the 15 kinds of boundary molecules are represented. For example, in an isolated T4 tail sheath as usually pictured, there are only two kinds of boundary molecules.

The condition of frame indifference restricts the form of the molecular free energies. We note first that, according to the definitions (3) and (9), the quantities $\mathbf{y}_1$ and $\mathbf{R}_1$ are transformed into $\mathbf{R}\mathbf{y}_1+\mathbf{c}$ and $\mathbf{R}\mathbf{R}_1$ under a superimposed rigid body motion $\mathbf{R}\mathbf{y}_i+\mathbf{c}$ of all the atoms. Thus, in the case of chains, the condition of frame indifference is (for interior molecules)

$$\psi(\mathbf{y}_1,\mathbf{R}_1,\mathbf{y}_2,\mathbf{R}_2)=\psi(\mathbf{R}\mathbf{y}_1+\mathbf{c},\mathbf{R}\mathbf{R}_1,\mathbf{R}\mathbf{y}_2+\mathbf{c},\mathbf{R}\mathbf{R}_2), \quad (15)$$

which must hold independently for $\mathbf{R},\mathbf{R}_1,\mathbf{R}_2\in\mathrm{SO}(3)$, and $\mathbf{c},\mathbf{y}_1,\mathbf{y}_2\in\mathbb{R}^3$. Making the special choice $\mathbf{R}=\mathbf{R}_1^T$ and $\mathbf{c}=-\mathbf{R}_1^T\mathbf{y}_1$, we see that

$$\psi(\mathbf{y}_1,\mathbf{R}_1,\mathbf{y}_2,\mathbf{R}_2)=\psi(0,\mathbf{I},\mathbf{R}_1^T(\mathbf{y}_2-\mathbf{y}_1),\mathbf{R}_1^T\mathbf{R}_2)=\varphi(\mathbf{t},\mathbf{Q}), \quad (16)$$

where $\mathbf{Q}=\mathbf{R}_1^T\mathbf{R}_2$ is a *relative orientation* that is unaffected by rigid body rotations and $\mathbf{t}=\mathbf{R}_1^T(\mathbf{y}_2-\mathbf{y}_1)$ is a *relative translation* which is also unaffected by superimposed rigid motions. Note that $\mathbf{Q}$ is not simply the rotation which maps the orientation of molecule 2 into that of molecule 1 (or vice versa), and similarly, $\mathbf{t}$ is not a simple translation of 2 into 1. Rather, these quantities behave like strains, and describe the six degrees of freedom associated with the straining of bond sites caused by changes of orientation and relative position of 1 and 2.

For sheets the restrictions of frame indifference are similar: the functions ψ_1 and ψ_2 in (14) both satisfy (16). We let $\varphi_{1,2}$ be the corresponding reduced functions defined by (16) subscripted by 1,2.

IV. COMPATIBILITY

Compatibility concerns the extent to which one can prescribe the quantities describing strain, or, more generally, the functions on which the free energy depends after the condition of frame indifference has been imposed. In our case this concerns the extent to which we can assign the relative translations and relative orientations.

In the case of chains we therefore assign $(\mathbf{t}_1,\mathbf{Q}_1,\ldots,\mathbf{t}_{N-1},\mathbf{Q}_{N-1})$ and ask whether there are positions and orientations $(\mathbf{y}_1,\mathbf{R}_1,\ldots,\mathbf{y}_N,\mathbf{R}_N)$ consistent with these in the sense that $\mathbf{t}_i=\mathbf{R}_i^T(\mathbf{y}_{i+1}-\mathbf{y}_i)$ and $\mathbf{Q}_i=\mathbf{R}_i^T\mathbf{R}_{i+1}$, $i=1,\ldots,N-1$. It is immediately seen that these conditions are solvable, and all solutions are related to each other by exact rigid motions of the entire molecule. Hence, the problem of compatibility for chains is analogous to the case of 1D rod theories in continuum mechanics: there are no conditions of com-

patibility and the freedom is precisely overall rigid deformations.

For sheets there are nontrivial restrictions of compatibility, as expected based on continuum shell theories. We begin by considering the case of four bonding directions. For the analysis below a *path* is a succession of nearest neighbors in $\mathcal{D}$ and a *loop* is a closed path. We assume here that $\mathcal{D}$ is discretely simply connected in the sense that every point is connected to every other point by a path and any non-self-intersecting closed loop in $\mathcal{D}\cap\mathbb{Z}^2$ is the boundary of the union of (closed) unit squares contained in $\mathcal{D}$. We assign relative translations and relative orientations

$$(\mathbf{t}_{i,j},\mathbf{Q}_{i,j}),\quad (i,j)\in\mathcal{D}^r,\quad \text{and } (\hat{\mathbf{t}}_{i,j},\hat{\mathbf{Q}}_{i,j}),\quad (i,j)\in\mathcal{D}^u, \tag{17}$$

where $\mathcal{D}^{r,u}$ are the subsets $(i,j)\in\mathcal{D}$ such that $(i+1,j)$ $[(i,j+1)]$ are also in $\mathcal{D}$ (r denotes "right" and u denotes "up"). We ask whether there are positions and orientations $\mathbf{y}_{i,j},\mathbf{R}_{i,j},(i,j)\in\mathcal{D}$, that satisfy

$$\mathbf{t}_{i,j}=\mathbf{R}_{i,j}^T(\mathbf{y}_{i+1,j}-\mathbf{y}_{i,j}),$$

$$\mathbf{Q}_{i,j}=\mathbf{R}_{i,j}^T\mathbf{R}_{i+1,j},\quad (i,j)\in\mathcal{D}^r,$$

$$\hat{\mathbf{t}}_{i,j}=\mathbf{R}_{i,j}^T(\mathbf{y}_{i,j+1}-\mathbf{y}_{i,j}),$$

$$\hat{\mathbf{Q}}_{i,j}=\mathbf{R}_{i,j}^T\mathbf{R}_{i,j+1},\quad (i,j)\in\mathcal{D}^u. \tag{18}$$

Immediately we see that there are some restrictions. For example, if $\mathbf{R}_{i,j}$ has been determined, then by successive application of $(18)_{2,4}$ there are overdetermined equations for, say, $\mathbf{R}_{i+1,j+1}$, these being

$$\mathbf{R}_{i+1,j+1}=\mathbf{R}_{i,j+1}\mathbf{Q}_{i,j+1}=\mathbf{R}_{i,j}\hat{\mathbf{Q}}_{i,j}\mathbf{Q}_{i,j+1},$$

$$\mathbf{R}_{i+1,j+1}=\mathbf{R}_{i+1,j}\hat{\mathbf{Q}}_{i+1,j}=\mathbf{R}_{i,j}\mathbf{Q}_{i,j}\hat{\mathbf{Q}}_{i+1,j}. \tag{19}$$

Equating these, we get

$$\hat{\mathbf{Q}}_{i,j}\mathbf{Q}_{i,j+1}=\mathbf{Q}_{i,j}\hat{\mathbf{Q}}_{i+1,j}, \tag{20}$$

or

$$\hat{\mathbf{Q}}_{i,j}\mathbf{Q}_{i,j+1}\hat{\mathbf{Q}}_{i+1,j}^T\mathbf{Q}_{i,j}^T=\mathbf{I}. \tag{21}$$

This has the following interpretation: as we go, say, clockwise around a unit square in the lattice $\mathbb{Z}^2$, the product of the $\mathbf{Q}$'s (taken with transpose if the path goes to the left or down) is the identity. Two neighboring squares, both traversed clockwise, give such identities of the form $\hat{\mathbf{Q}}_1\mathbf{Q}_2\hat{\mathbf{Q}}_3^T\mathbf{Q}_1^T=\mathbf{I}$ and $\hat{\mathbf{Q}}_3\mathbf{Q}_4\hat{\mathbf{Q}}_5^T\mathbf{Q}_3^T=\mathbf{I}$ which immediately gives $\mathbf{I}=\mathbf{Q}_1^T\hat{\mathbf{Q}}_1\mathbf{Q}_2\hat{\mathbf{Q}}_3^T\hat{\mathbf{Q}}_3\mathbf{Q}_4\hat{\mathbf{Q}}_5^T\mathbf{Q}_3^T=\mathbf{Q}_1^T\hat{\mathbf{Q}}_1\mathbf{Q}_2\mathbf{Q}_4\hat{\mathbf{Q}}_5^T\mathbf{Q}_3^T$, that is, $\hat{\mathbf{Q}}_1\mathbf{Q}_2\mathbf{Q}_4\hat{\mathbf{Q}}_5^T\mathbf{Q}_3^T\mathbf{Q}_1^T=\mathbf{I}$; this is a similar compatibility condition for the rectangle consisting of the union of the two squares. By induction and using the discrete simple connectedness[4] of $\mathcal{D}$, this extends to any non-self-intersecting closed loop in $\mathcal{D}\cap\mathbb{Z}^2$.

So far, the argument concerns the solution of the last two equations of (18). For the translations, by again traversing a unit square in the clockwise sense, we have from $(18)_{1,3}$ that $\mathbf{R}_{i,j}\hat{\mathbf{t}}_{i,j}+\mathbf{R}_{i,j+1}\mathbf{t}_{i,j+1}-\mathbf{R}_{i+1,j}\hat{\mathbf{t}}_{i+1,j}-\mathbf{R}_{i,j}\mathbf{t}_{i,j}=0$, which, after premultiplication by $\mathbf{R}_{i,j}^T$ gives

$$\hat{\mathbf{t}}_{i,j}+\hat{\mathbf{Q}}_{i,j}\mathbf{t}_{i,j+1}-\mathbf{Q}_{i,j}\hat{\mathbf{t}}_{i+1,j}-\mathbf{t}_{i,j}=\mathbf{0}. \tag{22}$$

As above, equations of this form for neighboring squares can be combined to an equation of compatibility for a rectangle and then, by iteration, to a non-self-intersecting closed loop.

By this time it is clear that the pattern of argument is essentially the same as that for differentials (i.e., this kind of argument does not really use that the differentials are small, if only nearest neighbors interactions are considered). That is, necessary and sufficient conditions for (17) to be compatible are that the compatibility conditions for unit squares in $\mathcal{D}$, i.e., all equations of the form

$$\hat{\mathbf{Q}}_{i,j}\mathbf{Q}_{i,j+1}\hat{\mathbf{Q}}_{i+1,j}^T\mathbf{Q}_{i,j}^T=\mathbf{I},$$

$$\hat{\mathbf{t}}_{i,j}+\hat{\mathbf{Q}}_{i,j}\mathbf{t}_{i,j+1}-\mathbf{Q}_{i,j}\hat{\mathbf{t}}_{i+1,j}-\mathbf{t}_{i,j}=\mathbf{0} \tag{23}$$

are satisfied. The necessity of these conditions has been proved above. The sufficiency follows by giving arbitrarily $\mathbf{y}_{0,0}\in\mathbb{R}^3,\mathbf{R}_{0,0}\in\mathrm{SO}(3)$, assuming without loss of generality that (0,0) is in $\mathcal{D}$. Then, for any other $(k,m)\in\mathcal{DB}$, we consider a path from (0,0) to (k,m). Successive application of Eq. (18) determines first $\mathbf{R}_{k,m}$ and then $\mathbf{y}_{k,m}$, and every such $\mathbf{R},\mathbf{y}$ along this path. By a process of exhaustion, i.e., construct a path which does not cross itself or any other path to a point whose values $\mathbf{R},\mathbf{y}$ have not been determined from a previously determined one, we then determine all values $\mathbf{R}_{i,j},\mathbf{y}_{i,j}$. These satisfy all of the equations (18). That is, by construction, a point (i,j) and neighbor $(i+1,j)$ $[(i,j+1)]$ are each connected to (0,0) by a path used in the construction. These paths may coincide over some initial length, but, once they depart from each other, they never intersect. Thus, by possibly shortening the loop, we can without loss of generality assume the paths form a non-self-intersecting loop with a single link removed. Satisfaction of (18) then holds as a consequence of the compatibility condition for such loops.

There is clearly also uniqueness of the construction of $\mathbf{R}_{i,j},\mathbf{y}_{i,j}$ up to the choice of $\mathbf{R}_{0,0},\mathbf{y}_{0,0}$, which, by the frame indifference of the quantities $\mathbf{Q},\mathbf{t}$ is equivalent to uniqueness up to overall rigid deformation.

Suppose now we add additional bonding directions. Since the equations (23) are both necessary and sufficient for the existence of the positions and orientations, and these positions and orientations are uniquely determined up to overall translation and rotation [which does not affect the $(\mathbf{t},\mathbf{Q})$'s],

[4]By the discrete simple connectedness of $\mathcal{D}$, a non-self-intersecting loop in $\mathcal{D}\cap\mathbb{Z}^2$ encloses a union of squares that can be completely exhausted by adding successive squares that share an edge.

then all values of $(\mathbf{t},\mathbf{Q})$ corresponding to other bonding directions are uniquely determined by $(\mathbf{t}_{i,j},\mathbf{Q}_{i,j}),(\hat{\mathbf{t}}_{i,j},\hat{\mathbf{Q}}_{i,j})$. One can write formulas for these. For example, if (as in the T4 sheath) we have the additional bonding directions $(i,j)-(i-1,j+1)$, then

$$\bar{\mathbf{t}}_{i,j} \overset{\text{def}}{=} \mathbf{R}_{i,j}^T(\mathbf{y}_{i-1,j+1}-\mathbf{y}_{i,j}) = \mathbf{Q}_{i-1,j}^T(\hat{\mathbf{t}}_{i-1,j}-\mathbf{t}_{i-1,j}),$$

$$\bar{\mathbf{Q}}_{i,j} \overset{\text{def}}{=} \mathbf{R}_{i,j}^T\mathbf{R}_{i-1,j+1} = \mathbf{Q}_{i-1,j}^T\hat{\mathbf{Q}}_{i-1,j}. \tag{24}$$

In summary, with additional bonding directions, necessary and sufficient conditions for compatibility are (23), together with the formulas of the type (24) that uniquely determine the values of $(\mathbf{t},\mathbf{Q})$ for these additional directions in terms of $(\mathbf{t}_{i,j},\mathbf{Q}_{i,j}),(\hat{\mathbf{t}}_{i,j},\hat{\mathbf{Q}}_{i,j})$.

V. HELICAL CONFIGURATIONS

As shown in Fig. 4 below, the tail sheath of bacteriophage T4 is a sheet consisting of the union of two families of helices. Helical structures arise often in biology and they also have special position within the context of the present theory, as we explain in this and the following sections.

From a purely geometric viewpoint Crane in 1950 [8] argued that if two proteins have complementary bonding sites and molecules bond at a specific angle, then chains of these molecules are likely to from helices. In nonlinear elasticity of rods and plates, helical configurations also arise in a natural way (Ericksen [9], Chouaieb and Maddocks [4], and Moakher and Maddocks [5]). In all of these arguments the frame-indifference of the free energy plays a central role, allowing the variables describing strain to be either constant (in rod theory) or else to depend on fewer reference coordinates for these special configurations.

We begin with chains and recall from (16) that the molecular free energy depends on relative translation and orientation $(\mathbf{t},\mathbf{Q})$. Motivated by the examples just cited we first try to figure out what are all configurations $(\mathbf{y}_1,\mathbf{R}_1,\ldots,\mathbf{y}_N,\mathbf{R}_N)$ having constant values of $(\mathbf{t},\mathbf{Q})$. In the following section we explain the energetic significance of this choice, beyond the obvious fact that such configurations have the property that the molecular free energy is independent of the molecule. This problem is immediately solved by the considerations of compatibility of the preceding section; we have to solve

$$\mathbf{R}_i^T(\mathbf{y}_{i+1}-\mathbf{y}_i)=\mathbf{t},\quad \mathbf{R}_i^T\mathbf{R}_{i+1}=\mathbf{Q},\quad i=1,\ldots,N-1, \tag{25}$$

and the general solution is

$$\mathbf{R}_{i+1}=\mathbf{R}_1\mathbf{Q}^i,\quad \mathbf{y}_{i+1}=\mathbf{y}_1+\mathbf{R}_1\sum_{j=0}^{i-1}\mathbf{Q}^j\mathbf{t},\quad i=1,\ldots,N-1, \tag{26}$$

where $\mathbf{y}_1\in\mathbb{R}^3,\mathbf{R}_1\in \mathrm{SO}(3)$ are arbitrary, and they are also the values of position and orientation corresponding to molecule 1. It is clear from (26) that the choice $\mathbf{y}_1\in\mathbb{R}^3,\mathbf{R}_1\in \mathrm{SO}(3)$ also corresponds to an arbitrary superimposed rigid deformation of the whole array.

The positions of the molecules described by the equations (26) lie on a helix. To see this put $\mathbf{R}_1=\mathbf{I}$ and note that $\mathbf{Q}=\mathbf{I}$ corresponds to the degenerate case of a molecules spaced equally along a line all with the same orientation. So we assume henceforth that $\mathbf{Q}\neq\mathbf{I}$. Then $\mathbf{Q}$ has an axial vector, that is, a vector $\mathbf{e}\in\mathbb{R}^3$ whose direction is uniquely determined such that $\mathbf{Qe}=\mathbf{e}$. By suitable choice of the magnitude of $\mathbf{e}$, we can decompose $\mathbf{t}=\mathbf{t}^{\parallel}+\mathbf{t}^{\perp}$, $\mathbf{t}^{\perp}\cdot\mathbf{e}=0,\mathbf{t}^{\parallel}\|\mathbf{e}$; then the second of (26) becomes

$$\mathbf{y}_{i+1}=\mathbf{y}_1+i\mathbf{t}^{\parallel}+\sum_{j=0}^{i-1}\mathbf{Q}^j\mathbf{t}^{\perp}. \tag{27}$$

The last term in (27) can be further simplified. To do so, note that $\mathbf{Q}-\mathbf{I}$ is invertible on the plane perpendicular to $\mathbf{e}$ and define $\mathbf{r}$ by $(\mathbf{Q}-\mathbf{I})\mathbf{r}=\mathbf{t}^{\perp},\mathbf{r}\cdot\mathbf{e}=0$, so that $\mathbf{Qr}=\mathbf{r}+\mathbf{t}^{\perp}$. Now, iterate the latter to get the identity,

$$\mathbf{Q}^i\mathbf{r}=\mathbf{r}+\sum_{j=0}^{i-1}\mathbf{Q}^j\mathbf{t}^{\perp}. \tag{28}$$

Choosing the arbitrary translation $\mathbf{y}_1=\mathbf{r}$ (to put the origin on the axis of the helix) and eliminating the sum in (27) using (28) we have,

$$\mathbf{y}_{i+1}=i\mathbf{t}^{\parallel}+\mathbf{Q}^i\mathbf{r}, \tag{29}$$

which, accounting for the conditions $\mathbf{r}\cdot\mathbf{e}=0$ and $\mathbf{Qe}=\mathbf{e}$, is the equation of a helix. The orientations $\mathbf{R}_i$ of these helical configurations also vary in a regular way along the helix in a manner given by (26) and illustrated, for example, in Fig. 5.

The basic geometric information, like formulas for the pitch and radius of the helix in terms of the given information $(\mathbf{t},\mathbf{Q})$, can be read off from the formulas given in the preceding paragraph. In particular, if $\nu\geqslant 1$ is the smallest number such that $\mathbf{Q}^{\nu}=\mathbf{I}$, then the pitch is $\nu|\mathbf{t}^{\parallel}|$. The radius is $|(\mathbf{Q}-\mathbf{I})^{-1}\mathbf{t}^{\perp}|$, the inverse taken on the plane perpendicular to $\mathbf{e}$. This inverse is given by $(\mathbf{Q}-\mathbf{I})^{-1}=[-1/\mathrm{tr}(\mathbf{Q}-\mathbf{I})](\mathbf{Q}-\mathbf{I})^T$.

Below, we will observe that the relaxed configurations of extended or contracted T4 tail can be viewed as a collection of six helices, each with 24 molecules. To evaluate the positions and orientations of all these molecules from experimental data, it will be useful to understand how the orientations of the molecules on a helix can be varied independently from the shape of the helix. This is not immediately obvious from the formulas (26), but is easy to work out. First it is clear geometrically (and it can be shown from the formulas above) that if the shape of the helix is given, i.e., all of the $\mathbf{y}_i$, then assignment of the orientation of one of the molecules on the helix determines the orientations of all the others. Thus there is expected to be one free rotation matrix $\mathbf{R}$ to define this orientation. Given a helical configuration defined by $(\mathbf{y}_1,\mathbf{R}_1,\mathbf{Q},\mathbf{t})$, then all other helical configurations with the same positions are given by

$$(\mathbf{y}_1,\mathbf{R}_1\mathbf{R},\mathbf{R}^T\mathbf{Q}\mathbf{R},\mathbf{R}^T\mathbf{t}),\quad \mathbf{R}\in \mathrm{SO}(3). \tag{30}$$

To use this formula, one can think of beginning with a helix of the desired shape and then choosing $\mathbf{R}\in \mathrm{SO}(3)$ so that

$\mathbf{R}_1\mathbf{R}$ is the desired orientation of molecule 1 and all the others then follow.

For sheets there are similar kinds of helical configurations, having the shape of a ribbon bent and twisted into a helix. These are discussed below in Secs. VI and VIII.

VI. BACTERIOPHAGE T4 TAIL SHEATH

In this section we specialize the formulas given above to the T4 tail sheath. The first task is to describe the sheath in its extended and contracted configurations and identify the positions and orientations using experimental measurements.

The T4 tail sheath can be viewed as a protein sheet as defined above. We can think of a cylinder oriented vertically. The lowest annulus of the cylinder is a circle of six molecules. Each of these six molecules generates a right handed helical chain consisting of 23 molecules.[5] Hence, we will identify the molecules accordingly, $(\mathbf{y}_{i,j},\mathbf{R}_{i,j})$, $i=1,\ldots,6$, $j=1,\ldots,23$.

We work in the usual orthonormal basis $(\mathbf{e}_1,\mathbf{e}_2,\mathbf{e}_3)$ and without loss of generality we will choose the overall rotation and translation so that the axes of all the helices coincide with $\mathbf{e}_3$ and the first annulus lies in the $\mathbf{e}_1,\mathbf{e}_2$ plane. The first annulus is a circle (i.e., a degenerate helical chain). According the results in Sec. V, this case corresponds to the case where $\mathbf{t}=\mathbf{t}_0$ is perpendicular to the axis of $\mathbf{Q}$ and a little calculation shows that without loss of generality (by suitably rotating the six molecules about the $\mathbf{e}_3$ axis) we can assume

$$\mathbf{t}_0=(-\rho,0,0),\quad \mathbf{Q}_\theta=\begin{pmatrix}\cos\theta & -\sin\theta & 0\\ \sin\theta & \cos\theta & 0\\ 0 & 0 & 1\end{pmatrix}, \tag{31}$$

$\rho>0$, and the fact that the six molecules are equally spaced on the helix gives $\mathbf{Q}_\theta^6=\mathbf{I}\Rightarrow\theta=\pi/3$. Without loss of generality we write $\mathbf{y}_1=\rho(1/2,\sqrt{3}/2,0)$. The radius of the circle of positions is ρ.

Emanating from each of these six molecules is a helical chain whose first molecule has now a given position and orientation. According to results of Sec. V, we need to specify $(\mathbf{t},\mathbf{Q})$ for each of these chains. In fact all of these chains have the same $(\mathbf{t},\mathbf{Q})$ because suitable rigid rotations and translations bring them into coincidence with each other: the whole configuration of the tail sheath has sixfold symmetry. The axis of $\mathbf{Q}$ is again $\mathbf{e}_3$ so $\mathbf{Q}$ has the form $(31)_2$, $\mathbf{Q}=\mathbf{Q}_\gamma$. Thus, besides the radius ρ of the cylinder, we need to determine the four parameters

$$\gamma \quad\text{and}\quad \mathbf{t}=(\tau_1,\tau_2,\lambda). \tag{32}$$

For this purpose we first show that τ_1,τ_2 are determined by ρ and γ. Referring to Sec. V and using that the initial point is $\mathbf{y}_1=\rho(1/2,\sqrt{3}/2,0)$, we have from the equations $\mathbf{t}=\mathbf{t}^{\|}+\mathbf{t}^{\perp},(\mathbf{Q}-\mathbf{I})\mathbf{r}=\mathbf{t}^{\perp},\mathbf{r}=\mathbf{y}_1$ that $(\mathbf{Q}-\mathbf{I})\mathbf{y}_1=\mathbf{t}^{\perp}$, from which τ_1,τ_2 are given by

[5]Leiman *et al.* demonstrate [11] that the tail sheath consists of 23 annuli, rather than 24 as described in preceding papers. According to this work the missing annulus can now be ascribed to the baseplate, based on its detailed protein structure.

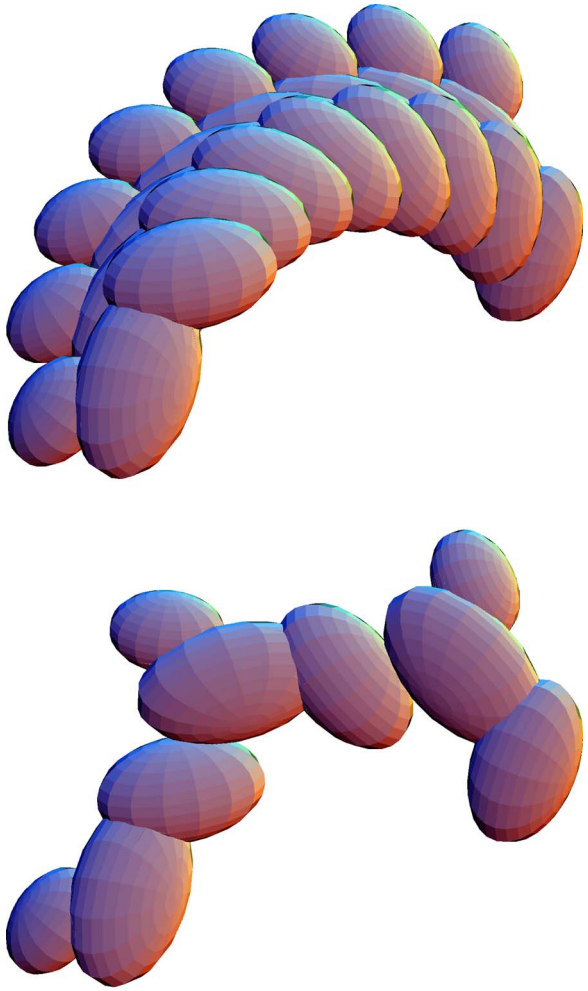

FIG. 2. (Color online) Illustration of the 8/3 rule of an extended sheath. Top: the first eight molecules $(i=1,j=1,\ldots,8)$ on the main helix, viewed down the axis of the cylinder. Bottom: the first three molecules $(i=1,2,3,j=1)$ on the first annulus, again viewed down the axis. The slight touching of domains of neighboring molecules on the bottom picture is an artifact of the ellipsoidal approximation; in reality these do not touch.

$$\tau_1=\frac{\rho}{2}[(\cos\gamma-1)-\sqrt{3}\sin\gamma],$$

$$\tau_2=\frac{\rho}{2}[\sin\gamma+\sqrt{3}(\cos\gamma-1)] \tag{33}$$

in terms of ρ and γ. It remains to determine ρ,λ, and γ. The values of these depend on whether we consider an extended or contracted sheath.

A. Extended tail sheath

Extended sheath has an interesting geometric property that we term the 8/3 rule. The rule is that the eighth molecule along one of these helices, beginning at a molecule on the first annulus, lies directly over the third molecule away counterclockwise along the annulus (Fig. 2). (The justification of this rule from measured data of Leiman *et al.* [11] is

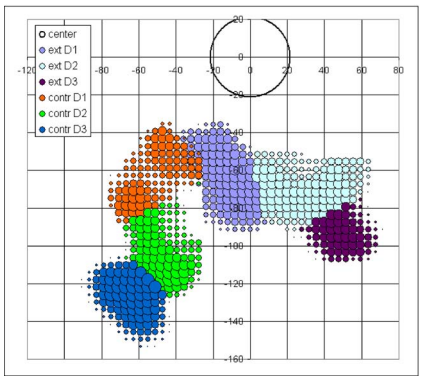

Extended Centers of Mass

	mass	x_1	x_2	x_3	radius
Domain 1	1679.22	-12.40	-64.14	42.32	65.32
Domain 2	1673.35	29.45	-70.08	49.13	76.02
Domain 3	751.18	49.25	-93.90	42.32	106.03
Total	4103.75	15.95	-72.01	45.10	73.75

Contracted Centers of Mass

	mass	x_1	x_2	x_3	radius
Domain 1	1683.34	-51.10	-63.54	45.71	81.53
Domain 2	2128.82	-46.08	-105.65	35.54	115.26
Domain 3	2408.94	-64.51	-126.87	40.94	142.33
Total	6221.10	-54.57	-102.47	40.38	116.10

FIG. 3. (Color online) Domain coordinates used to determine orientation $\mathbf{R}_{1,1}$. The circle denotes the centerline of the cylindrical sheath and each molecule is modeled by three domains. (The three domains to the right represents a molecule of extended sheath.) Total mass and center of mass of each domain are shown to the right.

given at the end of this section.) Specifically, in our notation,

$$\mathbf{y}_{1,8} \cdot \mathbf{e}_1 = \mathbf{y}_{3,1} \cdot \mathbf{e}_1, \quad \mathbf{y}_{1,8} \cdot \mathbf{e}_2 = \mathbf{y}_{3,1} \cdot \mathbf{e}_2. \tag{34}$$

This statement and the helical structure of the tail imply full periodicity, $\mathbf{y}_{(i,j+7)} \cdot \mathbf{e}_{1,2} = \mathbf{y}_{(i+2,j)} \cdot \mathbf{e}_{1,2}$ whenever these are defined. With regard to the present theory, all the good properties of helical configurations discussed above (and below) would hold without this "accidental" periodicity. This suggests that its presence is perhaps related to something other than the function of the tail, possibly its self-assembly via annulus-by-annulus epitaxial growth. In this regard, if one omits the last annulus, then the rest of the tail is exactly 1 period. In other words, without omissions, the 22nd annulus lies directly over the first annulus. It will be seen below that this 8/3 rule also applies to the orientation, $\mathbf{R}_{(1,8)} = \mathbf{R}_{(3,1)}$. This is of course the smallest period exhibited by the tail sheath. Possibly these facts are related to the process by which the tail tube directs the growth of the tail sheath, which is assembled in the extended form (below, the contracted form will not have this or a shorter period).

The two equations (34) give apparently two restrictions on the remaining parameters (ρ, λ, γ). Written out using Eq. (26), these two conditions are

$$-\sum_{j=0}^{6} \mathbf{Q}_\gamma^j \mathbf{t} + \mathbf{t}_0 + \mathbf{Q}_{\pi/3} \mathbf{t}_0 \parallel \mathbf{e}_3. \tag{35}$$

In fact this condition only involves γ and is equivalent to the pair of equations

$$2 + \cos 7\gamma - \sqrt{3} \sin 7\gamma = 0, \quad \sqrt{3} \cos 7\gamma + \sin 7\gamma = 0. \tag{36}$$

These equations have simultaneous roots at $\gamma = 2\pi/21 + 2\pi n/7$ where n is an integer. The root of interest (i.e., corresponding to a fraction of a turn in the counterclockwise sense) is $\gamma = 2\pi/21$. From the form of $\mathbf{t}$ it can now be seen that 21λ is the pitch of the helices.

It remains to prescribe the orientations of all the molecules. As explained in the few lines preceding Eq. (30) this is assignable independently of the positions. Since we have put $\mathbf{R}_1 = \mathbf{I}$, we may give this by giving the orientation of molecule (1,1), from which all the orientations of all the molecules are determined. In summary, the following information is needed from experiment for extended and contracted tail sheaths: (1) the orientation of molecule $(1,1) = \mathbf{R}_{1,1}$; (2) the radius of the cylinder of centers of masses $= \rho$; (3) the pitch of the helices $= 21\lambda$.

We obtained these from electron density maps of Leiman *et al.* [12] (we are grateful to Petr Leiman for the prepublication data on the extended sheath, without which the present theory would be incomplete). See the Appendix for how these data were used to represent the molecules. Briefly, these data do not give atom positions, but give an excellent picture of relatively rigid collections of atoms called domains. Both extended and contracted sheaths consist of three such domains. We assumed charge neutrality and computed centers of mass of domains, then used the formulas (3), (5), and (9) to compute the position and orientation. Three issues should be noted. (1) With three domains $\mathbf{F}$ is singular with rank equal to 2; nevertheless, $\mathbf{R}$ is uniquely determined by Eq. (9). (2) These data were rotated about the axis of the helix and translated into the position of molecule (1,1). This gives $\rho = 73.75$ Å, $\lambda = 40.6$ Å. We chose the extended sheath to be the reference configuration so that $\mathbf{R}_{1,1} = \mathbf{I}$. For a contracted sheath $\mathbf{R}_{1,1}$ is given by Eq. (39) below. (3) Note from Fig. 3 that masses of domains are not conserved. This is a consequence of the flexibility of certain bonds, which causes some mass to be lost by the averaging procedure inherent in any 3D reconstruction. To give definite results we ignored this problem and used the measured masses of each domain.

B. Contracted tail sheath

For the contracted tail sheath the evaluation is completely analogous to the above except that the 8/3 rule is replaced by a 12/1 rule,

$$\mathbf{y}_{1,12} \cdot \mathbf{e}_1 = \mathbf{y}_{1,1} \cdot \mathbf{e}_1, \quad \mathbf{y}_{1,12} \cdot \mathbf{e}_2 = \mathbf{y}_{1,1} \cdot \mathbf{e}_2. \tag{37}$$

As above this leads to a pair of equations for γ,

$$1 - \cos(11\gamma) + \sqrt{3} \sin(11\gamma) = 0,$$

$$\sqrt{3} - \sqrt{3} \cos(11\gamma) - \sin(11\gamma) = 0, \tag{38}$$

having a simultaneous first positive root at $\gamma = 2\pi/11$. As above, to complete the description, we need the orientation of the first molecule $\mathbf{R}_{1,1}$, the radius of the cylinder ρ, and the pitch of the helices, which in this case is 11λ. Using the electron density maps of Leiman *et al.* [11] in the same manner as above, we get for the contracted sheath $\rho = 116.1$ Å, $\lambda = 16.4$ Å, and

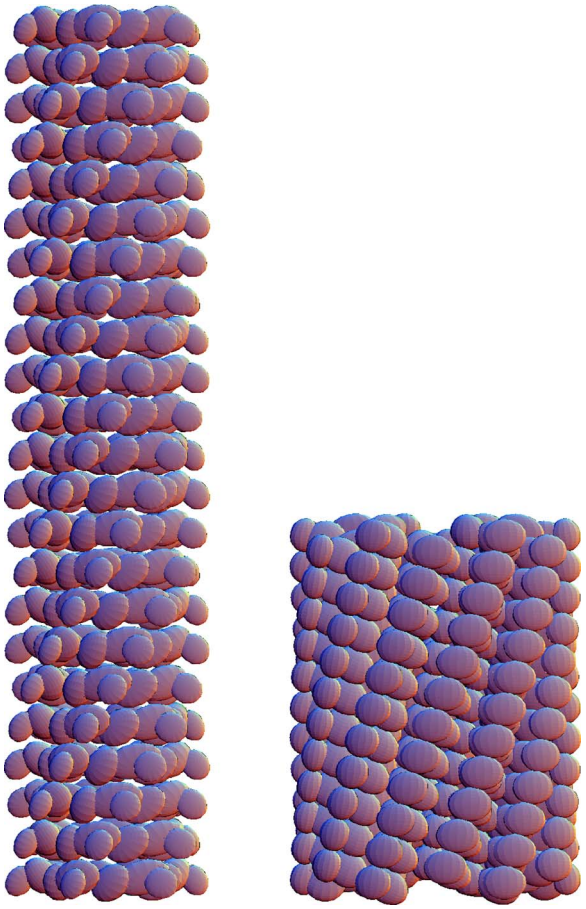

FIG. 4. (Color online) Pictures of extended and contracted tail sheaths based on the formula (40), using the method of visualization described in Sec. VI B.

$$\mathbf{R}_{1,1} = \begin{pmatrix} 0.426 & 0.4388 & -0.791 \\ -0.4378 & 0.8653 & 0.244 \\ 0.7916 & 0.242 & 0.561 \end{pmatrix} \tag{39}$$

In summary, the configuration of extended or contracted tail sheath is given by the following equations:

$$\mathbf{R}_{i,j} = \mathbf{Q}_{\pi/3}^{i-1}\mathbf{Q}_{\gamma}^{j-1}\mathbf{R}_{1,1},$$

$$\mathbf{y}_{i,j} = \mathbf{y}_1 + \sum_{k=0}^{i-2} \mathbf{Q}_{\pi/3}^{k}\mathbf{t}_0 + \mathbf{Q}_{\pi/3}^{i-1}\sum_{k=0}^{j-2} \mathbf{Q}_{\gamma}^{k}\mathbf{t},$$

$$i = 1, \ldots, 6, \quad j = 1, \ldots, 23, \tag{40}$$

where $\gamma = 2\pi/21$ for extended and $\gamma = 2\pi/11$ for contracted tail sheaths. Here, $\mathbf{Q}_\theta, \mathbf{t}_0$ are defined by Eq. (31), $\mathbf{y}_1 = \rho(1/2, \sqrt{3}/2, 0)$, $\mathbf{t}_0 = (-\rho, 0, 0)$, $\mathbf{t} = \lambda\mathbf{e}_3 + (\mathbf{Q}_\gamma - \mathbf{I})\mathbf{y}_1$, and we use the convention $\mathbf{Q}_\gamma^0 = \mathbf{I}$ (also, sums of the form $\Sigma_{k=0}^m$ where $m < 0$ are simply put equal to zero). Pictures of extended and contracted tail sheath obtained from formulas (40) with the data given above are shown in Fig. 4. The method of visualization is to approximate the domains of the molecules of extended and contracted sheaths by ellipsoids, centered at the centers of mass of the domains, as described in detail in the Appendix. As can be seen there, this is quite an accurate representation of the molecule. Then we applied the formulas (40) to this collection.[6]

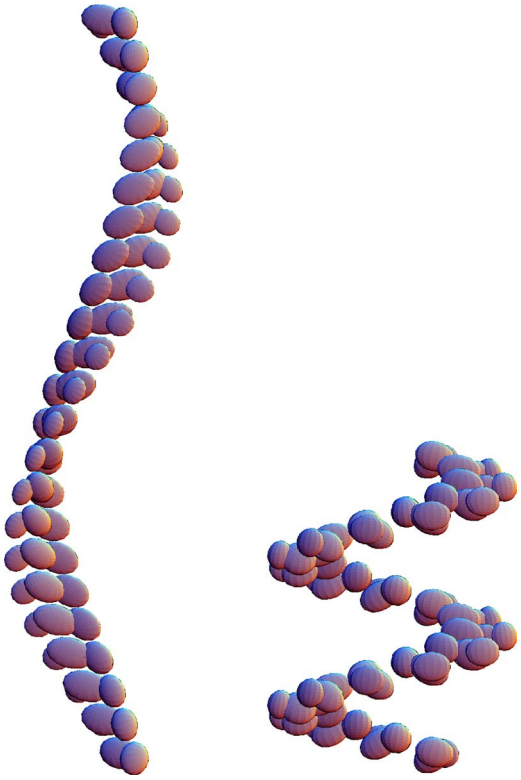

FIG. 5. (Color online) The main helix of the T4 tail sheath in extended and contracted forms, illustrating the screw action.

There is a substantial screw action that occurs when the sheath fully contracts. This can be seen from Fig. 5 which shows the corresponding main right handed helices in extended and contracted sheath. If the baseplate is held fixed during contraction, the neck experiences almost a full turn, the angle change being about 343°.

We should add that the data of Leiman *et al.* [11] also provide a direct measure of the validity of the 8/3 and 12/1 rules, which we have used above to evaluate $\gamma = 2\pi/21 = 17.14°$ and $\gamma = 2\pi/11 = 32.73°$, respectively. The direct measurement of Leiman *et al.* gives the very nearby values $\gamma = 17.2°, 32.9°$.

VII. A SIMPLE CONSTRAINED THEORY FOR BACTERIOPHAGE T4 TAIL SHEATH

A. Constraints

Our general expression for the free energy (14) of a protein sheet can be quite complicated, and in our case is made more complicated by the presence of additional bonding di-

[6]Note that the formulas (40) can be applied with accuracy to any model of the molecule, including the all-atom distribution. However, it is worth noting that the striking simplicity of (40) follows the precise definitions of position and orientation we have chosen; other kinematic descriptions may not give such simple formulas.

rections, as we explain below. In this section we use the known configurations of the sheath to make simplifying assumptions that allow us to arrive at a manageable form of the energy.

First we note that each molecule in the sheath undergoes a substantial motion. Nevertheless, there are some simplifying features of this motion. These features are remarkably close to the ideas of Pauling [13], who, prior to any knowledge of the T4 tail sheath, theorized that arrays of the helices of Crane could contract by having adjacent turns of the helix form bonds. Later, in his study of the T4 tail sheath, Moody [15] observed that bonds on the right handed helix remained to some extent invariant during contraction. He noticed that, on the main helix, while there is a substantial relative rotation of molecules, the distance between neighbors does not change too much. This concerns[7] neighboring molecules of the form $(i,j),(i,j+1)$, shown, e.g., for $i=1$ in Fig. 5. According to our Eq. (40) we have for both extended and contracted sheaths that this distance is $|\mathbf{t}|=|\mathbf{R}_{i,j}^{T}(\mathbf{y}_{i,j+1}-\mathbf{y}_{i,j})|$; it is of course independent of both i and j and is given by

$$|\mathbf{t}|^2=\lambda^2+2\rho^2(1-\cos\gamma). \tag{41}$$

When this is evaluated for extended and contracted sheaths using the data above we get, respectively, $|\mathbf{t}|=46.2,67.4$ Å. While these are fairly close, Moody noticed that if, instead of using the separate radii of extended and contracted sheaths, one uses in both cases an effective radius of $\rho=\rho_{\text{eff}}=77.6$ Å, then $\sqrt{\lambda^2+2\rho_{\text{eff}}^2(1-\cos\gamma)}=46.7$ Å for both contracted and extended sheaths. The reason for the smaller-than-average effective radius presumably relates to the relative importance of the bonding of inner domains, which appear to be in contact in electron micrograph cross sections of the sheath at a radius near ρ_{eff}.

We remark that if we approximate $\cos\gamma$ by $1-(1/2)\gamma^2$ in the expression $\lambda^2+2\rho_{\text{eff}}^2(1-\cos\gamma)$, and also adjust the value of ρ_{eff} slightly to $\rho_{\text{eff}}=76.33$ Å, then we have the following simple quadratic condition:

$$\lambda^2+\gamma^2\rho_{\text{eff}}^2=\begin{cases}2170\ \text{Å}^2 & \text{for extended sheath}\\ 2170\ \text{Å}^2 & \text{for contracted sheath.}\end{cases} \tag{42}$$

In view of its physical interpretation, we assume (42) represents a special stiffness in the T4 tail sheath and we adopt it as a constraint for all values of λ and γ. Below we generalize it to distorted configurations.

The constraint (42) has an interesting consequence. To describe this, we first recall that according to macroscopic nonlinear elasticity, a uniformly twisted cylinder subject to zero axial force and free sides changes its diameter and also its length. The latter is referred to as the Poynting effect. It is generically a second order effect: the elongation goes as the square of the angle of twist of the cylinder; the elongation can be either positive or negative and it is typically positive (lengthening) for elastomeric materials. For uniform states of the T4 tail sheath, that is, states given by the formula (40) subject to the constraint (42), we have a very strong *first order* Poynting effect. That is because, by (40), the end angle measured from the extended configuration is 22γ while the height is 22λ.

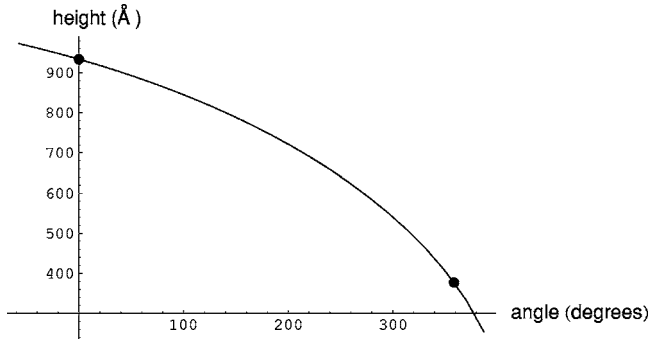

FIG. 6. Height of the tail sheath vs end angle (measured from extended sheath) according to the constraint, showing a strong first order Poynting effect. Dots correspond to extended and contracted sheaths.

Thus the theory predicts a height vs twist relation as shown in Fig. 6. This is essentially a plot of the constraint (42). Below in Sec. VII D, we show that a simplified explicit free energy has these uniform states as local minimizing free energy configurations subject to small axial torque and force near the extended or contracted states. We note that if the approximation $\cos\gamma\approx 1-(1/2)\gamma^2$ is not made, then, on the scale of Fig. 6, the resulting graph is indistinguishable from Fig. 6. Note the dramatic Poynting effect, particularly at contracted sheath. It would be interesting to look at this relationship experimentally.

There is another simplifying feature of the deformation of the T4 tail sheath that concerns the orientation. For molecule (1,1) the rotation that maps extended to contracted sheath is given in (39), and its axis is given by

$$(0.001,0.875,0.485). \tag{43}$$

The angle of rotation is close to 64.8°. Remarkably, the axis of rotation (43) is within about 1° of $(0,\sqrt{3}/2,1/2)$. A possible reason for this rotation and its implications become clear when we superimpose the rotation axis (black line) on pictures of a molecule (1,1) of an extended and contracted tail sheath (Fig. 7). From these pictures, if one thinks of the molecules as having the shape of a kind of twisted banana, then evidently the axis of rotation passes through its axis. Thus, the rotation of molecules of tail sheath seems largely constrained by steric hindrance. But there is another feature of this rotation that is suggested by the two pictures on the right of Fig. 7. In these two pictures we are looking directly down the axis of rotation. One can see that the rotation of (1,1) of about 60° is causing it to align itself approximately with the main helix. As above, this is consistent with the idea that there are strong bonds linking molecules on this helix that not only constrain lengths but also relative rotations. In fact, even though the molecules depicted at the right of Fig. 7 do not touch, there are strong bonds that link the innermost domains.

We now develop this idea quantitatively. To account for the evidence for steric hindrance, we assume that the orien-

[7]The relation between Moody's notation for bonds and ours is $AB=(i,j)(i,j+1)$, $AB'=(i,j)(i-1,j+1)$, $AC'=(i,j)(i-1,j+2)$.

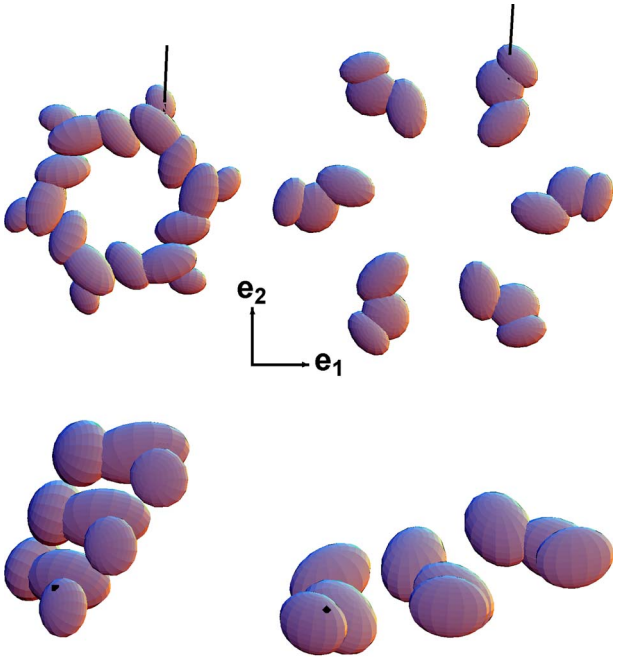

FIG. 7. (Color online) Left pair: the first annulus $(i=1,\ldots,6, j=1)$ of extended and contracted sheaths viewed down the axis of the cylinder, with the axis of the rotation of molecule 1 shown passing through its center of mass. Right pair: the first three molecules on the main helix $(i=1, j=1,2,3)$ of extended and contracted sheaths viewed parallel to the axis of rotation (shown as the black dot).

tation $\mathbf{R}_{1,1}$ has the fixed axis which we take to be $(0,\sqrt{3}/2,1/2)$, but we allow the angle of rotation to be free for the moment, i.e.,

$$\mathbf{R}_{1,1}(\theta)=\begin{pmatrix} \cos\theta & \frac{1}{2}\sin\theta & -\frac{\sqrt{3}}{2}\sin\theta \\ -\frac{1}{2}\sin\theta & \frac{3}{4}+\frac{1}{4}\cos\theta & \frac{\sqrt{3}}{4}-\frac{\sqrt{3}}{4}\cos\theta \\ \frac{\sqrt{3}}{2}\sin\theta & \frac{\sqrt{3}}{4}-\frac{\sqrt{3}}{4}\cos\theta & \frac{1}{4}+\frac{3}{4}\cos\theta \end{pmatrix}. \tag{44}$$

Guided by the pictures on the right of Fig. 7 and the motivation above, we compute $\mathbf{R}_{1,1}^T(\theta)(\mathbf{y}_{1,2}-\mathbf{y}_{1,1})$ for extended and contracted sheaths using Eq. (44) and the corresponding measured values of $\theta=0,64.8°$, respectively. The two vectors obtained are fairly close to each other as is expected based on Fig. 7. However, this computation reveals that the projection of these two vectors on the 1 axis is exceptionally close. That is, $\mathbf{e}_1\cdot\mathbf{R}_{1,1}^T(\theta)(\mathbf{y}_{1,2}-\mathbf{y}_{1,1})$ has nearly the same value of −21.2 Å for extended and contracted tail sheaths. We again hypothesize that this represents a special stiffness in this system, and we adopt it as a constraint, $\mathbf{e}_1\cdot\mathbf{R}_{1,1}^T(\theta)(\mathbf{y}_{1,2}-\mathbf{y}_{1,1})=-21.2$ Å. Written out using Eqs. (44) and (40), this constraint is

$$2\rho\cos\theta(1+\sqrt{3}\sin\gamma-\cos\gamma)+\sin\theta[\rho\sin\gamma+\rho\sqrt{3}\cos\gamma-\sqrt{3}(2\lambda+\rho)]=84.8\ \text{Å}. \tag{45}$$

It is natural to use this constraint to solve for θ, effectively making the orientation of each molecule slave to the variables that describe the spatial positions of the sheath. This is always possible for a wide range of reasonable values of γ,ρ,λ satisfying the earlier constraint (42). Some care has to be exercised with uniqueness, since generically (45) has a pair of solutions θ; however, only one of these lies in a modestly expanded interval containing [0,64.8°].

For uniform states, i.e., configurations obtainable using the formula (40), the constraints (42) and (45) reduce the energy to a function of the kinematic variables ρ and γ, effectively, radius and twist. It would be natural now to write the energy as a double-well energy in ρ,γ, with wells appropriate to contracted and extended sheaths. However, it is advantageous to consider also distorted states, so that the process of transformation can be described.

B. Nonuniform states

To describe nonuniform states, we first notice that our basic formula (40) is still useful. In fact, this formula can be used to describe an arbitrarily distorted sheath, by simply allowing $\rho,\gamma,\lambda,\mathbf{R}_{1,1}$ to depend on (i,j). To see this, we notice that if the molecule (i,j) occupies a certain position and has a certain orientation, then one can always find a helical cylinder with molecule (i,j) in the given position and with the given orientation. Effectively, the formula (40) with variables ρ,γ,λ defines certain helical coordinate system based on the structure of the T4 sheath. We note that this generalization changes somewhat the geometric interpretations given above of the variables $\rho,\gamma,\lambda,\mathbf{R}_{1,1}$.

In a setting of this generality, one could make a reasonable extrapolation of what should be the constraints, based on the stiffnesses of the main helix discussed above, but the resulting 276 degrees of freedom would still be rather large; once the energy of the T4 sheath becomes known quantitatively, it will then be worthwhile doing something like this, since general configurations and forces could be then computed using standard nonlinear optimization techniques. For the present, we make a 1D ansatz that positions and orientations are the same on each annulus, that is,

$$(\mathbf{y}_{i,j},\mathbf{R}_{i,j}) \text{ is given by Eq. (40) with } \rho=\rho_j,\ \gamma=\gamma_j,\ \lambda=\lambda_j,$$
$$\mathbf{R}_{1,1}=\mathbf{R}_j,\quad i=1,\ldots,6,\quad j=1,\ldots,23. \tag{46}$$

Our first goal is to reformulate the constraints in terms of these variables. We begin with the first constraint (42). If we calculate $|\mathbf{t}|=|\mathbf{R}_{i,j}^T(\mathbf{y}_{i,j+1}-\mathbf{y}_{i,j})|$ using (46) we see that it depends in a somewhat complicated way on j, but we can also see from the expressions that there is a natural change of variables that restores the simplicity of the expressions for uniform states. That change of variables is

$$\bar{\gamma}_j=j(\gamma_{j+1}-\gamma_j)+\gamma_j,\quad \bar{\lambda}_j=j(\lambda_{j+1}-\lambda_j)+\lambda_j,\quad j=1,\ldots,22. \tag{47}$$

The inverse mapping is simple averaging:

$$\gamma_j=\frac{1}{j-1}(\bar{\gamma}_1+\cdots+\bar{\gamma}_{j-1}),\quad \lambda_j=\frac{1}{j-1}(\bar{\lambda}_1+\cdots+\bar{\lambda}_{j-1}),$$

$$j = 2, \ldots, 23. \tag{48}$$

Note that for uniform states, $\bar{\gamma}_j = \gamma_j = \gamma$ and $\bar{\lambda}_j = \lambda_j = \lambda$. When the expression $|\mathbf{t}|^2 = |\mathbf{R}_{i,j}^T(\mathbf{y}_{i,j+1} - \mathbf{y}_{i,j})|^2$ is evaluated for 1D states in these new variables, it becomes

$$\rho_j^2 - 2\rho_j\rho_{j+1}\cos\bar{\gamma}_j + \rho_{j+1}^2 + \bar{\lambda}_j^2, \tag{49}$$

and the connection with (41) is immediately clear. In fact, it is expected based on the definition of $\bar{\gamma}_j$ that the approximation $\cos\bar{\gamma}_j \approx 1 - (1/2)\gamma_j^2$ is still reasonable and then (49) becomes $(\rho_{j+1} - \rho_j)^2 + \rho_{j+1}\rho_j\bar{\gamma}_j^2 + \bar{\lambda}_j^2$. Comparing with (42), it is natural to again replace all the ρ_j by the effective radius ρ_{eff}. We therefore adopt in the nonuniform case the constraint

$$\bar{\lambda}_j^2 + \bar{\gamma}_j^2\rho_{\text{eff}}^2 = 2170\ \text{Å}^2, \tag{50}$$

where $\rho_{\text{eff}} = 76.33$ Å.

Now we generalize the constraints (44) and (45) on the orientation. First, we recall that our way of writing the formula (40) automatically adjusts the orientation of each molecule on the sheath in a consistent way (preserving the helices) in response to a change of $\mathbf{R}_{1,1}$. Since we assumed above that $\mathbf{R}_{1,1}$ has the same axis for extended and contracted sheath, then we assume this remains true for nonuniform states and $\mathbf{R}_{1,1}$ continues to have the form (44) with θ replaced by θ_j.

Once again, the change of variables (47) proves to be extremely useful, for if we now calculate the quantity $\mathbf{e}_1 \cdot \mathbf{R}_{i,j}^T(\mathbf{y}_{i,j+1} - \mathbf{y}_{i,j}) = \mathbf{e}_1 \cdot \mathbf{R}_j^T(\mathbf{y}_{i,j+1} - \mathbf{y}_{i,j})$, we get

$$\frac{1}{4}\{-2\cos\theta_j(\rho_j + \rho_{j+1}\sqrt{3}\sin\bar{\gamma}_j - \rho_{j+1}\cos\bar{\gamma}_j) - \sin\theta_j[\rho_{j+1}\sin\bar{\gamma}_j + \rho_{j+1}\sqrt{3}\cos\bar{\gamma}_j - \sqrt{3}(2\bar{\lambda}_j + \rho_j)]\}, \tag{51}$$

with the obvious relation to (45). We therefore adopt the following constraint on orientation in the nonuniform case:

$$2\cos\theta_j(\rho_j + \rho_{j+1}\sqrt{3}\sin\bar{\gamma}_j - \rho_{j+1}\cos\bar{\gamma}_j) + \sin\theta_j[\rho_{j+1}\sin\bar{\gamma}_j + \rho_{j+1}\sqrt{3}\cos\bar{\gamma}_j - \sqrt{3}(2\bar{\lambda}_j + \rho_j)] = 84.8\ \text{Å}. \tag{52}$$

We again view this as a way to determine θ_j, $j = 1, \ldots, 22$, making the orientation slave to the other variables.

In summary, there is a natural expression of the constraints within the context of the 1D ansatz, this being (50)–(52); no internal contradictions arise, and there is freedom to make a variety of distorted states that interpolate between contracted and extended sheaths. The unconstrained kinematic variables can be taken to be local twist and radius, which for distorted states turn out to be $\bar{\gamma}_1, \ldots, \bar{\gamma}_{23}$ and $\rho_1, \ldots, \rho_{23}$. If these variables are subject to a simple interpolation between extended and contracted sheath, by defining

$$\bar{\gamma}_j = \mu(j)(2\pi/21) + [1 - \mu(j)](2\pi/11),$$

$$\rho_j = \mu(j)73.75\ \text{Å} + [1 - \mu(j)]\,116.1\ \text{Å}, \tag{53}$$

where, for example, $\mu(j)$ is a simple "tanh" transition layer, $\mu(s) = \frac{1}{2}\{\tanh[(s - j_0)/w] + 1\}$, then one can exhibit a contracting sheath as is shown in Fig. 8. These pictures are produced in this way, using the constraints (50) and (52) to determine the λ_j and θ_j and then placing all in the formula (40), as directed by (46). All three of these pictures have the same interfacial width $w = 1.5$ and interfacial positions $j_0 = 4, 12, 20$, respectively. These are not necessarily equilibrium states, as the computation of these would depend on a quantitative knowledge of the energy function, which we do not yet know.

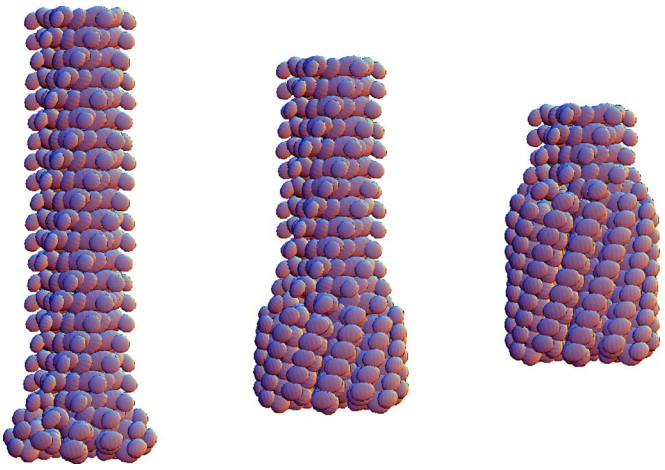

FIG. 8. (Color online) Deformations of tail sheaths satisfying the constraints and exhibiting transformation. See text.

These pictures are interesting from the point of view of nucleation. One of the important issues (raised in [16], where related references can be found) is that the T4 tail sheath is at a scale that would seem to suppress the martensitic phase transformation. Briefly, the argument is the following. In order to have a phase transformation with a distortion one expects an interface to pass through the body having a transition layer between phases. But because of the scaling between bulk and interfacial energy, the interfacial energy should dominate at sufficiently small scales, and, therefore, in a sufficiently small body, one would necessarily pay more free energy for the transition layer than the lowering of free energy due to the presence of the new phase. In the present case "interfacial" and "bulk" energies are better thought of as line and surface energies, but the argument is similar. Thus, nucleation is expected to be an important issue for phase transitions at small scales, and this is particularly true in the present case in view of the enormous transformation strain of the T4 tail sheath. It is known from the work of Moody that transformation begins at the baseplate. The distortion of the first annulus upon nucleation can be seen in Fig. 8. An alternative view is seen in Fig. 9 which shows a view from below; in this figure the lowest annulus is nearly fully transformed ($j_0 = 4$) on the left while the corresponding untransformed sheath is shown on the right.

Finally, a brief remark about constraints and frame indifference. It is well known that internal constraints in mechanical systems should be frame indifferent, and this may not be obvious in the present case. In (40) there is some freedom of how one assigns a change of frame, attributing this either to changes of $\gamma, \rho, \lambda, \mathbf{R}_{1,1}$ or, for example, to changes of $\mathbf{Q}_\gamma$ (at constant γ), $\mathbf{Q}_{\pi/3}, \mathbf{t}_0, \mathbf{t}, \mathbf{y}_1, \mathbf{R}_{1,1}$. The latter is preferred, and

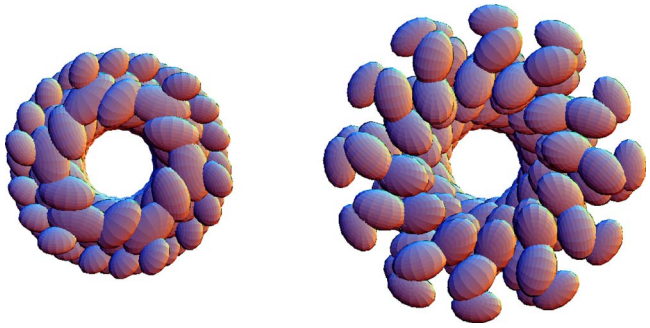

FIG. 9. (Color online) Nucleation of the phase transformation in the T4 sheath as viewed from below. Left: extended sheath. Right: view of sheath with the first annulus fully transformed, as in the leftmost picture of Fig. 8.

also preserves the 1D ansatz. The precise form of a change of frame $\mathbf{y}\to\mathbf{R}y+\mathbf{c}$, $\mathbf{R}\in \mathrm{SO}(3)$ is then $\mathbf{Q}_\gamma\to\mathbf{R}\mathbf{Q}_\gamma\mathbf{R}^T$, $\mathbf{Q}_{\pi/3}\to\mathbf{R}\mathbf{Q}_{\pi/3}\mathbf{R}^T$, $\mathbf{t}_0\to\mathbf{R}\mathbf{t}_0,\mathbf{t}\to\mathbf{R}\mathbf{t}$, $\mathbf{y}_1\to\mathbf{R}\mathbf{y}_1+\mathbf{c}$, $\mathbf{R}_{1,1}\to\mathbf{R}\mathbf{R}_{1,1}$. With this understanding, γ,ρ,λ are objective scalars and the constraints are frame indifferent.

C. Free energy

Having reduced the complexity of the energy by formulating constraints for a 1D ansatz, we are now in the position to suggest a relatively simple form of the energy function for nonuniform states of the form (46). We take the independent variables to be $\bar{\gamma}_1,\ldots,\bar{\gamma}_{23}$ and $\rho_1,\ldots,\rho_{23}$. In the extended T4 tail sheath the main helix is the only direction of strong bonding; however, in the contracted sheath there are three bonding directions, as identified by Moody [15] and Leiman *et al.* [12]. These are the bonds $(i,j)-(i,j+1)$, $(i,j)-(i-1,j+1)$, $(i,j)-(i-1,j+2)$. For this bonding the free energy is a minor generalization of (14):

$$\begin{aligned}\Psi(\mathbf{y}_{1,1},\mathbf{R}_{1,1},\ldots,\mathbf{y}_{6,23},\mathbf{R}_{6,23}) &= \sum_{i\in\{1,\ldots,6\},j\in\{1,\ldots,23\}} \psi_1(\mathbf{y}_{i,j},\mathbf{R}_{i,j},\mathbf{y}_{i,j+1},\mathbf{R}_{i,j+1}) \\ &\quad + \psi_2(\mathbf{y}_{i,j},\mathbf{R}_{i,j},\mathbf{y}_{i-1,j+1},\mathbf{R}_{i-1,j+1}) \\ &\quad + \psi_3(\mathbf{y}_{i,j},\mathbf{R}_{i,j},\mathbf{y}_{i-1,j+2},\mathbf{R}_{i-1,j+2}).\end{aligned} \tag{54}$$

Here we have omitted separate consideration of boundary molecules; to account for molecules beyond the boundaries, we do a suitable periodic extension. Recall that the ψ_1,ψ_2,ψ_3 depend on certain objective quantities, the $\mathbf{t}$'s and $\mathbf{Q}$'s [cf. Eq. (18)].

We assume the 1D ansatz (46) and the constraints (50)–(52). If we write out all of the frame-indifferent expressions appearing in the arguments of ψ_1 in the sum (54), we have

$$\mathbf{R}_{i,j}^T\mathbf{R}_{i,j+1}=f(\rho_j,\rho_{j+1},\bar{\gamma}_j),\quad \mathbf{R}_{i,j}^T(\mathbf{y}_{i,j+1}-\mathbf{y}_{i,j})=g(\rho_j,\rho_{j+1},\bar{\gamma}_j), \tag{55}$$

where f and g are somewhat complicated algebraic vector-valued functions. We recall that this bond (along the main helix) guides the assembly of the extended state and is preserved throughout contraction. Since this bond is relaxed in the extended state and undergoes relatively small deformations, one simple way to model it is as a harmonic function centered at the extended state:

$$\begin{aligned}\psi_1(\mathbf{y}_{i,j},\mathbf{R}_{i,j},\mathbf{y}_{i,j+1},\mathbf{R}_{i,j+1}) &= \frac{1}{12}\begin{Bmatrix}\rho_j-\rho_e\\ \bar{\lambda}_j-\lambda_e\end{Bmatrix}\begin{bmatrix}k_1 & k\\ k & k_2\end{bmatrix} \\ &\quad\cdot\begin{Bmatrix}\rho_j-\rho_e\\ \bar{\lambda}_j-\lambda_e\end{Bmatrix}+k_3(\rho_{j+1}-\rho_j)^2\end{aligned} \tag{56}$$

where k and $k_i>0$ are constants, and ρ_e and γ_e are the values measured for the extended sheath. The term containing k_3 is suggested by the presence of ρ_j,ρ_{j+1} and the expectation that this energy is minimized by the uniform state: this term is somewhat like the terms of the energy of a liquid crystal.

The bond $(i,j),(i-1,j+1)$ spans between adjacent main helices. This bond is largely nonexistent in the extended sheath and its formation drives the contraction. However, the energy ψ_2 for this bond depends on the same set of variables $\rho_j,\rho_{j+1},\bar{\gamma}_j$ as for $(i,j),(i,j+1)$. The radius and pitch of adjacent turns of the main helix provide a measure of the second bond's state. If the adjacent turns are close to the contracted state then the bond is formed. For configurations where the helices are far apart the bond is essentially broken. And for configurations where the helices become very close there is a strong repulsion. Consistent with this we propose the potential

$$\begin{aligned}\psi_2(\mathbf{y}_{i,j},\mathbf{R}_{i,j},\mathbf{y}_{i-1,j+1},\mathbf{R}_{i-1,j+1}) &= \frac{1}{12}[1-k_4(\rho_j-\tilde{\rho}_c)^2 \\ &\quad - k_5(\rho_{j+1}-\rho_j)^2]\mathcal{L}(\bar{\lambda}_j),\end{aligned} \tag{57}$$

where

$$\mathcal{L}(\lambda)=\begin{cases}-a(c-\lambda)^2(c-3\tilde{\lambda}_c+2\lambda), & \lambda\le c\\ 0, & \lambda>c,\end{cases} \tag{58}$$

is similar in shape to a Lennard-Jones potential, except that it has a cutoff at c, where $\mathcal{L}$ and its first derivative vanish (it is continuously differentiable). This part of the energy depends on the parameters $\tilde{\rho}_c,\tilde{\lambda}_c,c,k_4,k_5,a$, which have the following interpretations. For $\lambda>c$ the energy contribution to ψ_2 vanishes (i.e., the bond is broken). The values $\tilde{\rho}_c,\tilde{\lambda}_c$ are the minimizing values of ρ,λ for ψ_2; in practice, we adjust these so that the measured values ρ_c,λ_c are absolute minimizers of the total energy. The value a is the bond dissociation energy; k_4 controls the stiffness of this bond with respect to changes of radius, and k_5 favors uniformity. The term containing k_5 multiples $\mathcal{L}$ so that the tendency toward uniformity is not in force when the bond is broken. The third bond $(i,j),(i-1,j+2)$ is similar to the second, in that it forms upon contraction. It spans two helices, so the third bond energy depends on the pitch and radius of the second nearest helix, and it involves the larger set of variables $\rho_j,\rho_{j+1},\rho_{j+2},\bar{\gamma}_j,\bar{\gamma}_{j+1}$.

We take it to have a simple form similar to that of the second bond,

$$\psi_3(\mathbf{y}_{i,j},\mathbf{R}_{i,j},\mathbf{y}_{i-1,j+1},\mathbf{R}_{i-1,j+1}) = \frac{1}{12}[1-k_4(\rho_j-\tilde{\rho}_c)^2-k_5(\rho_{j+1}-\rho_j)^2-k_6(\rho_{j+2}-\rho_j)^2 - k_7(\bar{\lambda}_{j+1}-\bar{\lambda}_j)^2]\mathcal{L}(\bar{\lambda}_j),$$

where $\mathcal{L}$ is as in (58). In principle, all of the parameters $\tilde{\rho}_c,\tilde{\lambda}_c,c,k_4,k_5,a$ are likely to differ for bonds 2 and 3, but we do not alter the notation to reflect that.

So, in summary, for the constrained sheet subject to the 1D ansatz, we write the total free energy

$$\Psi(\mathbf{y}_{1,1},\mathbf{R}_{1,1},\ldots,\mathbf{y}_{6,23},\mathbf{R}_{6,23}) = \sum_{j\in\{1,\ldots,23\}}\psi(\rho_j,\rho_{j+1},\rho_{j+2},\bar{\lambda}_j,\bar{\lambda}_{j+1}) \tag{59}$$

where the energy per annulus $\psi=6(\psi_1+\psi_2+\psi_3)$ and $k_\alpha>0$, $\alpha=1,\ldots,7$, $a>0$, $k_1k_2-k^2>0$, $\lambda_c<c<\lambda_e$. Note that, because of the presence of the cutoff, the values ρ_e,λ_e are always relative minimizers of the energy if (as we assume) the stiffness matrix in (56) is positive definite.

This energy favors uniform configurations for a suitably restricted domain and for ranges of the parameters expected to be physically interesting. Consider the domain (λ_j,ρ_j) where $\mathcal{L}<0$ and the prefactor of $\mathcal{L}$ is positive. Then a lower bound for the energy on this domain is obtained by putting $k_3=k_5=k_6=0$ and this bound is achieved by a uniform configuration that minimizes each term (the individual terms of the sum are minimized at the same uniform state). We use the notation

$$\phi(\rho,\lambda)=\psi(\rho,\rho,\rho,\lambda,\lambda) \tag{60}$$

for the energy per annulus of uniform states.

A simple explicit energy that uses all of the measured data that we have available, but otherwise makes somewhat arbitrary choices of constants, and has a relative minimizer at the extended state and an absolute minimizer at the contracted state, is obtained by putting $k_1=0.333$ zcal Å^{-2}, $k_2=3.0$ zcal Å^{-2}, $k=0$, $k_4=10^{-4}$ Å^{-2}, $a=0.3719$ zcal Å^{-3}, $c=30$ Å, $\tilde{\lambda}_c=13.3901$ Å, $\tilde{\rho}_c=161.398$ Å, and then by evaluating at a uniform state (1 zcal$=10^{-24}$ kcal). This gives the double-well energy pictured in Fig. 10. Here the choice of a reflects the calorimetric measurement of Arisaka, Engel, and Klump [17] that gives $\phi(\rho_e,\lambda_e)-\phi(\rho_c,\lambda_c)=60$ zcal/annulus, based on arguments described at the end of this subsection.

The tendency toward uniform states plays an important role during self-assembly of tail sheath. During assembly, the baseplate forces the first annulus to have the extended radius $\rho_1=\rho_e$. As subsequent annuli are added they do so as to match the radius of the annulus below. The second and third bonding directions remain incomplete, since the formation of these bonds would require the annuli to adopt the contracted radius. Proper assembly is accomplished by design; the penalty for mismatching a neighboring annulus outweighs the energy the could be liberated by forming the additional bonds. Our energy given above has the flexibility to model

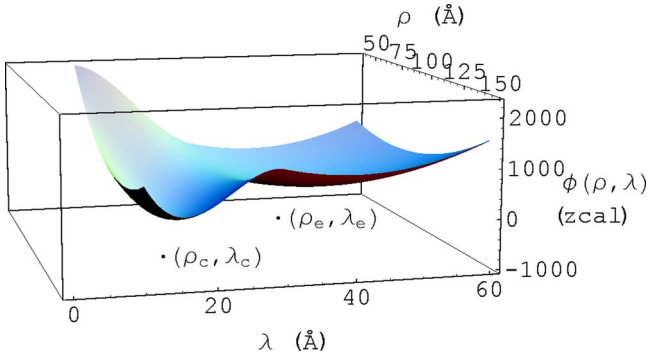

FIG. 10. (Color online) Special energy for tail sheath.

this behavior through two features: (1) the state (ρ_e,λ_e) is a minimizer of energy with respect to all uniform small perturbations of (ρ,λ), and (2) the terms involving k_3,k_5,k_6,k_7 can be tuned so that the addition of a new layer onto the growing extended sheet would be penalized from being added with (ρ,λ) near the contracted values, even though these have lower uniform energy. The complete analysis of self-assembly would require a molecule-by-molecule growth mechanism, involving boundary energies, but the present energetic considerations are expected to play a role.

For the rest of the paper we use a more general energy than the special form given above, but one that retains some of its essential features. That is we assume an energy per annulus of the form $\psi(\rho_j,\rho_{j+1},\rho_{j+2},\bar{\lambda}_j,\bar{\lambda}_{j+1})$ [cf. Eq. (59)] having the properties

$$\psi(\rho_c,\rho_c,\rho_c,\lambda_c,\lambda_c)<\psi(\rho_1,\rho_2,\rho_3,\lambda_1,\lambda_2) \quad \text{for all } (\rho_1,\rho_2,\rho_3,\lambda_1,\lambda_2) \text{ not equal to } (\rho_c,\rho_c,\rho_c,\lambda_c,\lambda_c),$$

$$\psi(\rho_e,\rho_e,\rho_e,\lambda_e,\lambda_e)<\psi(\rho_1,\rho_2,\rho_3,\lambda_1,\lambda_2) \quad \text{for all } (\rho_1,\rho_2,\rho_3,\lambda_1,\lambda_2) \text{ near, but unequal to, } (\rho_e,\rho_e,\rho_e,\lambda_e,\lambda_e),$$

$$\psi(\rho_c,\rho_c,\rho_c,\lambda_c,\lambda_c)<\psi(\rho_e,\rho_e,\rho_e,\lambda_e,\lambda_e). \tag{61}$$

For this more general energy we retain the notation $\phi(\rho,\lambda)=\psi(\rho,\rho,\rho,\lambda,\lambda)$, so it follows from the above that

$$\phi(\rho_c,\gamma_c)<\phi(\rho,\gamma) \quad \text{for all } (\rho,\gamma)\neq(\rho_c,\gamma_c),$$

$$\phi(\rho_e,\gamma_e)<\phi(\rho,\gamma) \quad \text{for all } (\rho,\gamma)\neq(\rho_e,\gamma_e) \text{ but near } (\rho_e,\gamma_e). \tag{62}$$

We make one other assumption on the height difference between the energy wells. In [17] Arisaka *et al.* did calorimetry on T4 tail sheaths with contraction triggered by two methods: raising the temperature to 72 °C and by increasing the concentration of urea. The former gave −44 kcal/mol (of gp18 molecules) whereas the latter gave −25 kcal/mol (of gp18 molecules). We use the former number here as it was considered the more accurate by these authors. From the details of the measurement, raising the temperature did not give

reversible contraction, but rather irreversible contraction, and temperatures higher than 72 °C caused denaturation of the whole sheath. Thus, one can infer that the free energy of contracted sheath is still lower than of extended sheath at 72 °C, though not as low as at 25 °C. Without any additional information and considering that at least spontaneous contraction occurred at 72 °C, we estimate the height difference between the wells by the following procedure. We restore the temperature dependence of ϕ and Taylor expand in the temperature, omitting the error terms,

$$\phi(\rho,\lambda,\theta_2) = \phi(\rho,\lambda,\theta_1) + \frac{\partial\phi(\rho,\lambda,\theta_1)}{\partial\theta}(\theta_2-\theta_1). \quad (63)$$

We put $\theta_1=25$ °C and $\theta_2=72$ °C, evaluate (63) at (ρ_e,λ_e) and (ρ_c,λ_c), and subtract, estimating $\phi(\rho_e,\lambda_e,\theta_2) \approx \phi(\rho_c,\lambda_c,\theta_2)$. Now, as is common in the interpretation of calorimetric measurements of phase transformations, we interpret the temperature times entropy difference as the latent heat:

$$\theta_2\left(\frac{\partial\phi(\rho_c,\lambda_c,\theta_1)}{\partial\theta} - \frac{\partial\phi(\rho_e,\lambda_e,\theta_1)}{\partial\theta}\right) = 440 \text{ zcal/annulus}. \quad (64)$$

Here we have ignored the temperature dependence of the entropy evaluated at either well separately. Combining Eqs. (63) and (64) we get that the entropy difference of the two phases is 1.27 zcal/K annulus and that

$$\phi(\rho_e,\lambda_e) - \phi(\rho_c,\lambda_c) = 60 \text{ zcal/annulus}. \quad (65)$$

D. Some simple uniform deformations and some relations between moduli

For the purpose of defining various moduli, it is convenient to introduce the free energy per unit reference length (the reference being the contracted state) by defining

$$\phi_c(\rho,\gamma) = \frac{1}{\lambda_c}\phi(\rho,\lambda). \quad (66)$$

Second derivatives of $\phi_c(\rho,\lambda)$ with respect to the pair (ρ,λ) have interpretations as various moduli. For example, if we consider small deformations about, say, the contracted sheath, then we write

$$\phi_c(\rho,\lambda) = \phi_c^0 + \frac{1}{2}[A(\rho-\rho_c)^2 + 2B(\rho-\rho_c)(\lambda-\lambda_c) + C(\lambda-\lambda_c)^2] + \cdots, \quad (67)$$

where ϕ_c^0 is the free energy per unit length of undistorted contracted sheath. We assume this form is positive definite.

We now interpret these moduli A,B,C. Working within the 1D ansatz, suppose we hold the annulus $j=1$ fixed and apply an axial force $\mathbf{f}=f\mathbf{e}_3$ to annulus $j=23$, treated as a dead load. Then the total energy of sheath and loading device is

$$\Psi(\mathbf{y}_{1,1},\mathbf{R}_{1,1},\ldots,\mathbf{y}_{6,23},\mathbf{R}_{6,23}) - \mathbf{y}_{1,23}\cdot\mathbf{f} = \Psi(\mathbf{y}_{1,1},\mathbf{R}_{1,1},\ldots,\mathbf{y}_{6,23},\mathbf{R}_{6,23}) - 22f\lambda_{23}. \quad (68)$$

[Recall the relation between λ_j and $\bar{\lambda}_j$, Eq. (48).] Using the assumptions (61) and the argument just preceding (60), we see that the minimizing state $\{\rho_1,\ldots,\rho_{23}\}$, $\{\bar{\lambda}_1,\ldots,\bar{\lambda}_{23}\}$ is uniform,

$$\rho_1 = \cdots = \rho_{23} = \rho, \quad \bar{\lambda}_1 = \cdots = \bar{\lambda}_{23} = \lambda, \quad (69)$$

and (ρ,λ) minimizes

$$\phi_c(\rho,\lambda) - f\frac{\lambda}{\lambda_c}. \quad (70)$$

Minimizing this expression over (ρ,λ) for small values of f, we get

$$\lambda-\lambda_c = \frac{A}{\lambda_c(AC-B^2)}f+\cdots,$$

$$\rho-\rho_c = \frac{-B}{\lambda_c(AC-B^2)}f+\cdots,$$

$$\gamma-\gamma_c = \frac{-A}{\rho_{eff}^2\gamma_c(AC-B^2)}f+\cdots. \quad (71)$$

The tensile modulus [i.e., the proportionality factor between f and $(22\lambda-22\lambda_c)/22\lambda_c$] is therefore

$$(\text{tensile modulus}) = \frac{\lambda_c^2(AC-B^2)}{A}. \quad (72)$$

Hence, due to the positive-definiteness of the quadratic form (67), tensile force produces extension, and also twist, with an end angle that decreases with increasing force. We expect $B>0$ in which case the Poisson effect is the usual one: lengthening produces a decrease in the radius. We can define a "Poisson's ratio" via the usual formula [−(radial strain)/(axial strain)]:

$$(\text{Poisson's ratio}) = \frac{\lambda_c}{\rho_c}\frac{B}{A}. \quad (73)$$

For simple torsion defined by the loading device energy $-22M\gamma$, where $M\mathbf{e}_3$ is the applied moment, energy minimization of $\phi_c - M(\gamma/\lambda_c)$, analogously to the above, leads to uniformity and to the equations

$$\gamma-\gamma_c = \frac{A\lambda_c}{\gamma_c^2\rho_{eff}^4(AC-B^2)}M+\cdots,$$

$$\rho-\rho_c = \frac{B}{\rho_{eff}^2\gamma_c(AC-B^2)}M+\cdots,$$

$$\lambda-\lambda_c = \frac{-A}{\rho_{eff}^2\gamma_c(AC-B^2)}M+\cdots. \quad (74)$$

From here, we identify

$$(\text{torsional modulus}) = \frac{(\text{moment})}{(\text{twist})/(\text{length})} = \frac{\gamma_c^2\rho_{eff}^4(AC-B^2)}{A}. \quad (75)$$

Thus we predict that the torsional modulus is proportional to the tensile modulus, the proportionality factor depending only on the geometry of the contracted sheath. In contrast, in macroscopic elasticity the torsional and tensile moduli are governed by different elastic constants (i.e., the shear and Young's moduli, respectively). This unusual behavior arises from our unusual constraints.

Finally, we briefly consider the resistance of protein structures to internal pressure. This may be relevant to the interactions between the sheath and tail tube, so in fact it is more related to the extended sheath (it is also of course highly relevant to the packaging of DNA in capsids [18]). For internal pressure p, the associated loading device energy is $23\lambda\pi\rho^2 p$. It is trivial to work out the associated moduli so we do not record that here.

What is more interesting is to work out the reaction forces. When a body is constrained, there should be reaction forces, that is, certain kinds of forces that do not produce deformation. In the present setting but in the fully nonlinear case, we consider a sheath subject to a tensile force f, a twisting moment M and an internal pressure p altogether, with an associated loading device energy $-22f\lambda - 22M\gamma + 22\lambda\pi\rho^2 p$. Taking the first variation of the energy with respect to (ρ,γ) we see that the resulting two equations do not uniquely determine the three unknowns (f,M,p). In fact it turns out that changes of p generically lead to deformation and the constraint force only involves f and M. The result can be stated in the following way. Suppose that the sheath is in equilibrium at a state $(\tilde{\rho},\tilde{\gamma})$ corresponding to generalized forces (f,M,p). Then, $(\tilde{\rho},\tilde{\gamma})$ is in equilibrium if (f,M) are changed to $(f+f_1,M+M_1)$, where

$$M_1 = -\frac{d\lambda}{d\gamma} f_1 = \frac{\rho_{eff}^2 \tilde{\gamma}}{\tilde{\lambda}} f_1. \tag{76}$$

Alternatively, this condition can be thought of in terms of work: changes of force and moment consistent with Eq. (76) do no work on the sheath.

We note that all the equilibrium states given here exhibit the strong Poynting effect discussed in Sec. VII A.

VIII. RELAXED STATES

It is interesting to contrast our theory of the protein sheet with nonlinear continuum theories of plates and shells. As a related example, the mechanical behavior of carbon nanotubes have been shown to conform to such continuum theories in many aspects, especially regarding elasticity and buckling [19]. The results given above arising from the constraints, especially the first order Poynting effect and the relations between elastic moduli, suggest differently, but these results are closely connected with the presence of the constraints. As we show here, the predictions of the unconstrained theory are also essentially different from continuum theories. This is not fundamentally a "nanoscale" phenomenon, but is related to the particular structure of protein sheet: compact globular proteins with local bonding and a sensitivity to orientation.

To review, nonlinear continuum theories of thin plates and shells come in various varieties, depending on the strength of the applied forces (for a rigorous treatment and an overview of the regimes, see [20]). For the largest applied forces there is membrane theory, defined in the following way. Let $\varphi(\mathbf{G})$ be the three-dimensional nonlinear elastic energy of the material expressed as a function of the deformation gradient $\mathbf{G}$. We suppose as usual that φ is frame indifferent, $\varphi(\mathbf{QG}) = \varphi(\mathbf{G})$ for all $\mathbf{Q} \in \mathrm{SO}(3)$, and that φ is minimized on SO(3). Let $(\mathbf{e}_1,\mathbf{e}_2,\mathbf{e}_3)$ be an orthonormal basis with $\mathbf{e}_3$ normal to the plate in its reference configuration, and write $\mathbf{G}=G_{ij}$ in this basis. To describe membrane theory we express the deformation gradient as its three column vectors, $\mathbf{G}=(\mathbf{y}_1|\mathbf{y}_2|\mathbf{y}_3)$. If $\mathbf{y}(x_1,x_2)$, $(x_1,x_2) \in S$, is the deformation of the plate then, in the absence of a loading device, the energy is

$$\int_S \varphi(\mathbf{y}_{,1}|\mathbf{y}_{,2}|\mathbf{b})\,dx_1 dx_2. \tag{77}$$

This is minimized over the independent fields $(\mathbf{y}(x_1,x_2),\mathbf{b}(x_1,x_2))$ ($\mathbf{b}$ describes deformations relative to the "middle surface"). Suppose that we have no boundary conditions imposed. Then, the energy in (77) is minimized by $(\mathbf{y},\mathbf{b})$ satisfying

$$\mathbf{y}_{,1} = \mathbf{R}(x_1,x_2)\mathbf{e}_1, \quad \mathbf{y}_{,2} = \mathbf{R}(x_1,x_2)\mathbf{e}_2,$$

$$\mathbf{b} = \mathbf{R}(x_1,x_2)\mathbf{e}_3, \quad \mathbf{R}(x_1,x_2) \in \mathrm{SO}(3). \tag{78}$$

The third of these equations simply determines $\mathbf{b}$, while the first two restrict the deformation. In fact, the first two of these equations define so-called *isometric mappings*. Isometric mappings are essentially the mappings that one can illustrate by taking a flat sheet of paper and deforming it, including the possibility of making folds and rather complex "crumpling." At the next level of approximation, for weaker forces, we have nonlinear bending theory. This is defined by the same kinematics as just described, but with the energy

$$\frac{1}{24}\int_S \psi((\nabla\mathbf{y})^T\nabla\,\mathbf{b})\,dx_1 dx_2, \tag{79}$$

where $\psi(\mathbf{G}) = \min_c q(G_{\alpha\beta} + c_\alpha \delta_{3\beta})$, $\delta_{\alpha\beta}$ is the Kronecker delta, and q is the quadratic form

$$q(\mathbf{H}) = \frac{\partial^2 \varphi(\mathbf{I})}{\partial F_{\alpha\beta}\partial H_{\gamma\delta}} H_{\alpha\beta} H_{\gamma\delta}. \tag{80}$$

In this case the energy (80) is minimized over isometric mappings *only*, i.e., over the solutions of (78). Thus, in summary, isometric mappings are the basic relaxed states of plate theories: they are the zero-energy deformations of membrane theory and the finite-energy deformations of bending theory. Shell theories are variants of the above in which the given reference state is generally curved. In that case the finite energy deformations are isometric mappings of the curved reference state.

What are the relaxed states of the present theory? To calculate the analog of the above, we should minimize the energy of the sheet

$$\Psi(\mathbf{y}_{1,1},\mathbf{R}_{1,1},\ldots,\mathbf{y}_{N,M},\mathbf{R}_{N,M}) = \sum_{(i,j)\in\mathbb{Z}^2\cap\mathcal{D}} \psi_1(\mathbf{y}_{i,j},\mathbf{R}_{i,j},\mathbf{y}_{i+1,j},\mathbf{R}_{i+1,j}) + \psi_2(\mathbf{y}_{i,j},\mathbf{R}_{i,j},\mathbf{y}_{i,j+1},\mathbf{R}_{i,j+1}), \tag{81}$$

without loading device energies or boundary conditions, over all positions and orientations. Here we have assumed two bonding directions and we have ignored boundary molecules. To simplify, this can be written (modulo possibly a few missing or additional boundary molecules)

$$\Psi = \sum_{(i,j)\in\mathbb{Z}^2\cap\mathcal{D}} \tilde{\psi}_1(\mathbf{t}_{i,j},\mathbf{Q}_{i,j}) + \tilde{\psi}_2(\hat{\mathbf{t}}_{i,j},\hat{\mathbf{Q}}_{i,j}), \tag{82}$$

but now it must be borne in mind that the independent variables $(\mathbf{t}_{i,j},\mathbf{Q}_{i,j},\hat{\mathbf{t}}_{i,j},\hat{\mathbf{Q}}_{i,j})$ are subject to the compatibility conditions (23). These conditions, repeated here,

$$\hat{\mathbf{Q}}_{i,j}\mathbf{Q}_{i,j+1}\hat{\mathbf{Q}}_{i+1,j}^T\mathbf{Q}_{i,j}^T = \mathbf{I},$$

$$\hat{\mathbf{t}}_{i,j} + \hat{\mathbf{Q}}_{i,j}\mathbf{t}_{i,j+1} - \mathbf{Q}_{i,j}\hat{\mathbf{t}}_{i+1,j} - \mathbf{t}_{i,j} = \mathbf{0}, \tag{83}$$

couple molecules (i,j) with $(i+1,j)$ and $(i,j+1)$. Clearly, we cannot (as we did above) minimize (82) by minimizing the "integrand" $\tilde{\psi}_1(\mathbf{t}_{i,j},\mathbf{Q}_{i,j})+\tilde{\psi}_2(\hat{\mathbf{t}}_{i,j},\hat{\mathbf{Q}}_{i,j})$, for this would typically give a minimizer, say, of the form

$$\mathbf{t}_{i,j} = \mathbf{t},$$

$$\mathbf{Q}_{i,j} = \mathbf{Q},$$

$$\hat{\mathbf{t}}_{i,j} = \hat{\mathbf{t}},$$

$$\hat{\mathbf{Q}}_{i,j} = \hat{\mathbf{Q}},$$

where

$$\tilde{\psi}_1(\mathbf{t},\mathbf{Q}) \leqslant \tilde{\psi}_1(\mathbf{a},\mathbf{R}) \quad \text{for all } (\mathbf{a},\mathbf{R}),$$

$$\tilde{\psi}_2(\hat{\mathbf{t}},\hat{\mathbf{Q}}) \leqslant \tilde{\psi}_2(\hat{\mathbf{a}},\hat{\mathbf{R}}) \quad \text{for all } (\hat{\mathbf{a}},\hat{\mathbf{R}}), \tag{84}$$

and it is seen that such a minimizer would generically fail the compatibility conditions, which in this case become

$$\hat{\mathbf{Q}}\mathbf{Q}\hat{\mathbf{Q}}^T\mathbf{Q}^T = \mathbf{I},$$

$$\hat{\mathbf{t}} + \hat{\mathbf{Q}}\mathbf{t} - \mathbf{Q}\hat{\mathbf{t}} - \mathbf{t} = \mathbf{0}. \tag{85}$$

One can consider more complex rearrangements of the sum (82), with different "integrands," but the analogous problem arises again. For example, the apparently most promising rearrangement is the sum[8]

$$\Psi = \sum_{\substack{(i,j)\in\mathbb{Z}^2\cap\mathcal{D}\\ i+j=\text{even}}} \tilde{\psi}_1(\mathbf{t}_{i,j},\mathbf{Q}_{i,j}) + \tilde{\psi}_2(\hat{\mathbf{t}}_{i,j},\hat{\mathbf{Q}}_{i,j}) + \tilde{\psi}_1(\mathbf{t}_{i,j+1},\mathbf{Q}_{i,j+1}) + \tilde{\psi}_2(\hat{\mathbf{t}}_{i+1,j},\hat{\mathbf{Q}}_{i+1,j}). \tag{86}$$

Here the summand contains exactly the independent variables appearing in the constraints, and therefore we could minimize it with respect to all values of the independent variables subject to the constraints. But one then sees that the solution actually satisfies only the compatibility conditions on every other cell and generically does not give a minimizer.

In discrete theory the impossibility of minimizing the energy for each bond individually is termed *frustration*. In continuum theory the concept is similar [21]: it is the inability of minimizers of the energy density to satisfy conditions of compatibility inherent in the kinematics.[9] We can say that our sheet is also frustrated, in the sense that minimization of the energy density for each bond does not generically give a compatible deformation. Here, the word "generically" means that, even if these compatibility conditions happen to be (accidentally) satisfied for a minimizer, then they are not satisfied if $\tilde{\psi}_1$ or $\tilde{\psi}_2$ are smoothly perturbed consistent with all of their assumed symmetries. As indicated above, even if we allow small collections of multiple bonds and minimize the energy of these, subject to constraints of compatibility, we also obtain a configuration that is not compatible in the large.

In biology, unlike materials science, there is the phenomenon of evolution of materials to achieve fitness. Thus for a protein sheet, there might be reasons, for example, to achieve a particularly low energy state, for a protein sheet to be nongeneric. Thus it is of interest to assume that $\mathbf{t},\mathbf{Q}$ and $\hat{\mathbf{t}},\hat{\mathbf{Q}}$ minimize, respectively, $\tilde{\psi}_1,\tilde{\psi}_2$ and also satisfy (85) and then to see what kinds of sheets emerge. We call such states *fully relaxed states*: each bond is relaxed and the configuration is compatible.

To calculate all fully relaxed states, we merely have to characterize all solutions of (85) and then calculate the implied positions and orientations. This is a straightforward algebraic exercise and we just give the results. First, a useful characterization of the solutions of (85) is the following. Each solution falls into one of the categories below.

(1) $\mathbf{Q}$ and $\hat{\mathbf{Q}}$ are coaxial, $\mathbf{Qe}=\hat{\mathbf{Q}}\mathbf{e}=\mathbf{e}, |\mathbf{e}|=1$, and

(a) If $\mathbf{Q}\neq\mathbf{I}$ and $\hat{\mathbf{Q}}\neq\mathbf{I}$, then $\mathbf{t}=\mathbf{t}_1+\tau\mathbf{e}$ and $\hat{\mathbf{t}}=\hat{\mathbf{t}}_1+\hat{\tau}\mathbf{e}$ for some $\tau,\hat{\tau}$ with $\mathbf{t}_1\cdot\mathbf{e}=\hat{\mathbf{t}}_1\cdot\mathbf{e}=0$, and $\hat{\mathbf{t}}_1=(\mathbf{I}-\mathbf{Q})^{-1}(\mathbf{I}-\hat{\mathbf{Q}})\mathbf{t}_1$, the inverse taken on the plane perpendicular to $\mathbf{e}$.

(b) If $\mathbf{Q}\neq\mathbf{I}$ and $\hat{\mathbf{Q}}=\mathbf{I}$, then $\mathbf{t}$ is arbitrary but $\hat{\mathbf{t}}=\tau\mathbf{e}$ for some τ.

(c) If $\mathbf{Q}=\mathbf{I}$ and $\hat{\mathbf{Q}}\neq\mathbf{I}$, then $\hat{\mathbf{t}}$ is arbitrary but $\mathbf{t}=\tau\mathbf{e}$ for some τ.

(d) If $\mathbf{Q}=\mathbf{I}$ and $\hat{\mathbf{Q}}=\mathbf{I}$, then $\hat{\mathbf{t}}$ and $\mathbf{t}$ are arbitrary.

[8] We ignore possible problems with this rearrangement near the boundary.

[9] A simple example of frustration in continuum theory is illustrated by the energy $\int_{\mathcal{D}}|\nabla z-\mathbf{Ax}|^2 d\mathbf{x}$, where $\mathbf{A}$ is a nonsymmetric matrix. In this case there is a unique smooth minimizer but it is not obtained by minimizing the integrand.

(2) $\mathbf{Q}=-\mathbf{I}+2\mathbf{e}\otimes\mathbf{e}$ and $\hat{\mathbf{Q}}=-\mathbf{I}+2\hat{\mathbf{e}}\otimes\hat{\mathbf{e}}$, $|\mathbf{e}|=|\hat{\mathbf{e}}|=1,\mathbf{e}\cdot\hat{\mathbf{e}}=0$, and

(a) $\hat{\mathbf{t}}=\tau_1\mathbf{e}+\tau(\mathbf{e}\times\hat{\mathbf{e}})$, $\mathbf{t}=\tau_2\hat{\mathbf{e}}+\tau(\mathbf{e}\times\hat{\mathbf{e}})$ for some τ_1,τ_2,τ.

Now, using these results we go back and compute the uniquely determined (up to overall rigid body motion) positions and orientations. For simplicity we assume an $N\times M$ sheet. We find, in all cases,

$$\mathbf{R}_{i+1,j+1}=\mathbf{R}_{1,1}\mathbf{Q}^i\hat{\mathbf{Q}}^j,$$

$$\mathbf{y}_{i+1,j+1}=\mathbf{y}_{1,1}+\mathbf{R}_{1,1}\left(\sum_{k=0}^{j-1}\hat{\mathbf{Q}}^k\hat{\mathbf{t}}+\hat{\mathbf{Q}}^j\sum_{k=0}^{i-1}\mathbf{Q}^k\mathbf{t}\right),$$

$$i=1,\ldots,N,\quad j=1,\ldots,M. \tag{87}$$

But this is exactly of the form of (40) for the T4 tail sheath. Recall that in the formula for the tail sheath the $\mathbf{R}_{1,1}$ was moved through the $\mathbf{Q}^i\hat{\mathbf{Q}}^j$ using the remark given at the end of Sec. V.

It is intriguing to ponder whether these fully relaxed states are actually realized by the tail sheath (or other protein sheets) and, if so, the implications of this with regard to stability and evolutionary development. Of course, with the various choices of $\mathbf{t},\mathbf{Q},\hat{\mathbf{t}},\hat{\mathbf{Q}}$ as enumerated above, the sheet will not look exactly like a tail sheath. We explored this numerically by choosing various cases and found that the general appearance is, however, much like a tail sheath; in fact, it can be proved from the formula (87) that the bonding direction $(i,j)-(i-1,j+1)$ is also a helix[10] (with translation $\mathbf{Q}(\hat{\mathbf{t}}+\mathbf{t})$. Figure 11 shows a generic picture of a fully relaxed state, with the molecule represented by a simple ellipsoid.

To complete this story, we make brief remarks about the remaining cases of the enumeration above. In item 1, if either $\mathbf{Q}=\mathbf{I}$ or $\hat{\mathbf{Q}}=\mathbf{I}$ then the appearance is still more or less like Fig. 11, but one family of helices degenerates to straight lines of molecules that are parallel to the axis of the cylinder. If both $\mathbf{Q}=\mathbf{I}$ and $\hat{\mathbf{Q}}=\mathbf{I}$, then the cylinder degenerates to a planar sheet, with crystalline symmetry, and parallel orientations of molecules. Finally, item 2 is a bit surprising; it describes a collection of four molecules, not generally at the corners of a regular tetrahedron, but such that each pair of the molecules is twinned, that is, individuals of the pair are related by a 180° rotation.

In summary, our theory of a protein sheet is generically frustrated. Energy minimizers are generally naturally curved, as in shell theories, but this curvature is determined by the energy. Isometric mappings seem to play no role here. In our theory if one considers energy densities $\tilde{\psi}_1,\tilde{\psi}_2$ that are minimized at compatible pairs $(\mathbf{t},\mathbf{Q}),(\hat{\mathbf{t}},\hat{\mathbf{Q}})$ (i.e., fully relaxed states) then the energy minimizers look much like the tail sheath of bacteriophage T4 and are given by simple formulas.

[10]Apparently, the formula produces helical configurations in all rational directions of $\mathbb{Z}^2$.

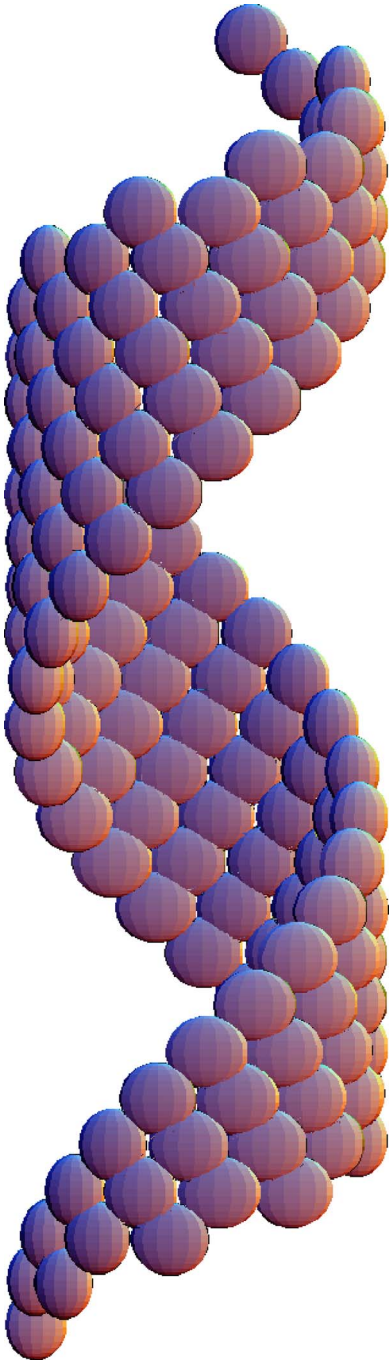

FIG. 11. (Color online) A generic fully relaxed state.

IX. EXPERIMENTS SUGGESTED BY THE THEORY

We have noted above several places above where there are possible experimental tests of our predictions. These include the extension-twist relation (Fig. 6), the linearized behavior near contracted or extended sheath (72)–(75), and the reaction forces that preserve deformation (76). We now discuss two other types of predictions that relate directly to biological and interesting nonbiological behavior.

A. The force of penetration

One of the most important predictions of our model is the force of penetration. Consider applying an axial force f to

contracted sheath, so as to stress-induce the transformation to extended sheath. Alternatively, one can imagine applying sufficient tension to extended sheath to just prevent contraction, i.e., the stall force. We neglect the interactions with the tail tube, assuming it to be weakly bonded to the sheath even when it is in the extended state, as is thought to be true [22,12]. For small values of f the behavior is given by the analysis of (68)–(72), and we expect the initial slope of the force-elongation curve [f vs $(\lambda-\lambda_c)/\lambda_c$] given by the modulus $\lambda_c^2(AC-B^2)/A$. There is expected to be significant nonlinearity of the response, because the constraints themselves are nonlinear. The details of the response near transition may depend on details of the loading device—whether hard or soft, for example—but one expects some kind of load drop on nucleation. The transformation is expected to take place via movement of an interface, as pictured qualitatively in Fig. 8 and at approximately constant free energy, because a bias of free energy toward either phase would, by energy minimization, tend to drive out the interface, one way or the other. This suggests the criterion

$$\Psi(\mathbf{y}^c,\mathbf{R}^c)-22f\lambda_{23}^c=\Psi(\mathbf{y}^e,\mathbf{R}^e)-22f\lambda_{23}^e, \tag{88}$$

where the uniform states $(\mathbf{y}^{c,e},\mathbf{R}^{c,e})=(\mathbf{y}_{1,1}^{c,e},\mathbf{R}_{1,1}^{c,e},\ldots,\mathbf{y}_{6,23}^{c,e},\mathbf{R}_{6,23}^{c,e})$ are assumed to be in equilibrium. Let superscripted variables $(\lambda^{e,c},\rho^{e,c},\gamma^{e,c})$ be associated with these uniform equilibrium states. Using the special form of the energy (62)–(66), we get

$$\phi_c(\rho^c,\lambda^c)-f(\lambda^c/\lambda_c)=\phi_c(\rho^e,\lambda^e)-f(\lambda^e/\lambda_c), \tag{89}$$

where

$$\frac{\partial\phi_c(\rho^{c,e},\lambda^{c,e})}{\partial\rho}=0,\quad \frac{\partial\phi_c(\rho^{c,e},\lambda^{c,e})}{\partial\lambda}=\frac{f}{\lambda_c}. \tag{90}$$

Solving these together, we get

$$\begin{aligned} f=f_{trans}&=\frac{[\phi_c(\rho^e,\lambda^e)-\phi_c(\rho^c,\lambda^c)]\lambda_c}{(\lambda^e-\lambda^c)}\\ &=\frac{[\phi_c(\rho_e,\lambda_e)-\phi_c(\rho_c,\lambda_c)]}{(\lambda_e/\lambda_c-1)}\\ &\quad+O\left(\max_{c,e}\frac{A_{c,e}}{A_{c,e}C_{c,e}-B_{c,e}^2}f^2\right). \end{aligned} \tag{91}$$

The error term depends also on geometric factors and can be written explicitly, but we note that it is of the form [f^2/(tensile modulus)]. Thus, if $f\ll$(tensile modulus) then this term is negligible as compared to f, and the force at transformation is a simple ratio of the height difference between the energy well minima at extended and contracted sheath and the difference between the lengths of the sheath. These kinds of results are well known in the study of phase transformations.

Of course, the virus uses the reverse transformation, from extended to contracted sheath, during penetration. The maximum force available for penetration is expected to be also f_{trans}.

We can evaluate the force of contraction based on the height difference between the wells, accounting for the reservations given at the end of Sec. VII C. Combining Eqs. (91) and (65), we get,

$$f_{trans}=103\ \text{pN}. \tag{92}$$

By comparison, the stall force measured by laser tweezers during DNA packaging in $\phi 29$ was 57 pN [1]. We would tend to think that the number 103 is a lower estimate for the actual force, because $\Delta\phi$ is underestimated at 72 °C as explained in Sec. VII C. If we divide this force by the cross-sectional area of the sheath to get a stress, we get about 0.5 MPa. This is quite low as a (maximum) transformation stress in a macroscopic crystalline martensitic material. However, the transformation strain in the T4 sheath is enormous, so, if we calculate the energy density of contraction based on these numbers, we get numbers that are comparable to those measured in the best shape memory materials, which themselves exhibit the highest energy densities in any known actuator system [23].

The transformation can also be induced by applying a pure axial moment. This leads to the analog of (88)–(91), except using the loading device energy $-22M\gamma$, and gives the moment at transformation of

$$\begin{aligned} M=M_{trans}&=\frac{[\phi_c(\rho^e,\lambda^e)-\phi_c(\rho^c,\lambda^c)]\lambda_c}{(\gamma^e-\gamma^c)}\\ &=\frac{[\phi_c(\rho_e,\lambda_e)-\phi_c(\rho_c,\lambda_c)]\lambda_c}{\gamma_e-\gamma_c}\\ &\quad+O\left(\max_{c,e}\frac{A_{c,e}}{A_{c,e}C_{c,e}-B_{c,e}^2}M^2\right). \end{aligned} \tag{93}$$

Neglecting the higher order terms in (91) and (93) we have the simple approximate relationship between the forces and moment needed to cause transformation in the sheath:

$$f_{trans}\approx\frac{\gamma_e-\gamma_c}{\lambda_e-\lambda_c}M_{trans}=-\frac{1}{89\ \text{Å}}M_{trans}. \tag{94}$$

B. Biomolecular epitaxy, patterning and devices

In this section we explore some more speculative ideas. T4 tail sheath is a kind of biomolecular actuator, and one could imagine that it could function as part of a manmade machine [24] that could interact in an intimate way with biological organisms. Tubes of *polysheath* several micrometers long have been synthesized [25,26]; polysheath is similar to, but not exactly the same as, contracted sheath. Tubes of extended sheath have not been synthesized separate from the baseplate and tail tube, and this is understandable in view of their higher free energy and also the possible role of the baseplate in stabilizing the extended sheath via epitaxy.

One basic interesting line of thought is to consider the possibility of changing the heights of the energy wells. As is true in a great many biological systems, hydrophobicity plays a critical role, and this can be appreciated in the present case by looking at Fig. 4. There, it is clear by inspection that extended sheath exposes substantially more surface area to the surrounding solution than contracted sheath, and this qualitatively explains its higher free energy. But it also indi-

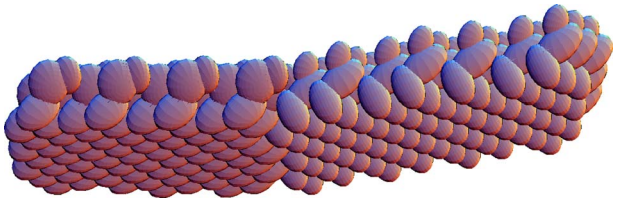

FIG. 12. (Color online) Edge-on view, slightly below horizontal, of the interface between contracted (left) and extended (right) sheath.

cates that the relative free energies of the extended and contracted sheaths are amenable to adjustment via manipulation of the solution chemistry. Systematic studies [26] of the effect of solution chemistry on the breakup of parts of the virus (capsid, neck, tail sheath, tail tube, baseplate, tail fibers) demonstrate sensitivity to solution chemistry. Apparently, solutions that cause a contracted tail sheath to extend have not yet been found. However, if by this means one could exchange the heights of the wells, then tail sheath would be like a shape memory material. In a highly schematic way, one could alter the solution so that extended sheath is stable. Then one could add an axial tensile force to the sheath. Again manipulating the solution, one could return it to phage-physiological conditions and, if the force was not too large [i.e., below the value f_{trans} of (91)] then the sheath would transform to the contracted form, while doing work on the force. This would be a machine that converts chemical free energy of the solution to mechanical energy. The very small cross section of the sheath would allow it to target a small region of a cell. One could consider the possibility of vast arrays of these tubes. In this regard, we note that ordered planar arrays of whole viruses have been deposited on surfaces (not using epitaxy) by Lee *et al.* [27].

In the following discussion we allow rather drastic changes of the sheath, but we enforce the constraints (42) and (45), these being in our view fundamental to its behavior. The T4 sheath is in the shape of a cylinder, but it is interesting to think about the possibility of slitting along a generator and unrolling it. We first note that it is possible to do this without violating the constraints. Second, the extended tail sheath exhibits an epitaxial relation to the baseplate, and this likely plays a role in self-assembly of the sheath during formation and subsequent stabilization. Thus we suggest the possibility of growing films of tail sheath epitaxially. In general, epitaxial growth is aided by a substrate with the same lattice parameters as the sheath, that is

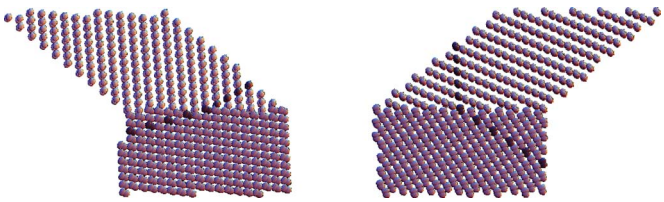

FIG. 13. (Color online) The two compatible interfaces that separate extended (above) from contracted (below) sheath. In each case the dark line of atoms was the main helix before unrolling the sheath.

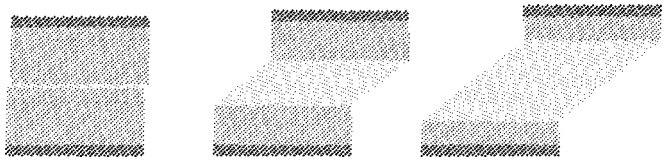

FIG. 14. Shear-inducing the transformation from contracted to extended sheath. Drawn with the lattice parameters of extended and contracted sheaths but with molecules represented by dots. The molecules are released from the substrate except for the two dark strips at the top and bottom of the sheet.

also chemically compatible with the sheath. The most likely possibility is to grow the lower free energy contracted form (see the left of Fig. 13 below, which shows the epitaxial surface). It is interesting to note that epitaxial growth of protein sheets could possibly take advantage of the shapes of molecules and the presence of functional groups, in addition to the matching of lattice parameters and use of surface chemistry, the latter principles familiar from the epitaxial growth of semiconductors.

While it does not violate the constraints, unrolling is a pretty drastic distortion, so one can expect some deviation of the lattice vectors from the values $\mathbf{t}_0^{c,e}, \mathbf{t}^{c,e}$ of Sec. VI. Nevertheless, in the analysis below, we do use those values, together with the orientations $\mathbf{R}_{1,1}^{c,e}$. Without loss of generality (using frame indifference) we first rotate these vectors into the 1,2 plane (we do not relabel the resulting vectors) and we apply the same rotations to the orientations. We plot the sheet as $i\mathbf{t}_0+j\mathbf{t}$ where i and j are integers.

The transformation matrix $\mathbf{G}$ that maps $\mathbf{t}_0^c, \mathbf{t}^c$ into $\mathbf{t}_0^e, \mathbf{t}^e$ is the matrix

$$\begin{pmatrix} 0.053 & -1.088 \\ 0.999 & 1.543 \end{pmatrix}. \tag{95}$$

By direct calculation $\mathbf{G}^T\mathbf{G}$ has eigenvalues 2.06, 0.567. As is known from the theory of martensitic transformations in sheets,[11] the fact that these values straddle 1 (i.e., $2.06 > 1 > 0.567$) means that there are exactly two interfaces on the sheet where extended and contracted sheet meet compatibly. These are pictured in Fig. 13. We have rotated the sheets suitably so that the interfaces are horizontal. The original orientation can be inferred from the dark lines of atoms, which correspond to what was the main helix (cf. Fig. 5) before unrolling. A cross section of the interface on the right is seen in Fig. 12.

Note that on the left of Fig. 13 the dark line of atoms is approximately in the direction of the interface. This reflects the constraint, which embodies the idea that the two phases are approximately equally stretched along this line. The reason that this line does not exactly coincide with the interface is related to the use of the effective radius, rather than the actual radius, in Eq. (42). As mentioned above, the values of

[11] See, e.g., [29] which shows how to calculate these lines and the corresponding deformations. The presence of these two interfaces was first noticed by Olson and Hartman [7].

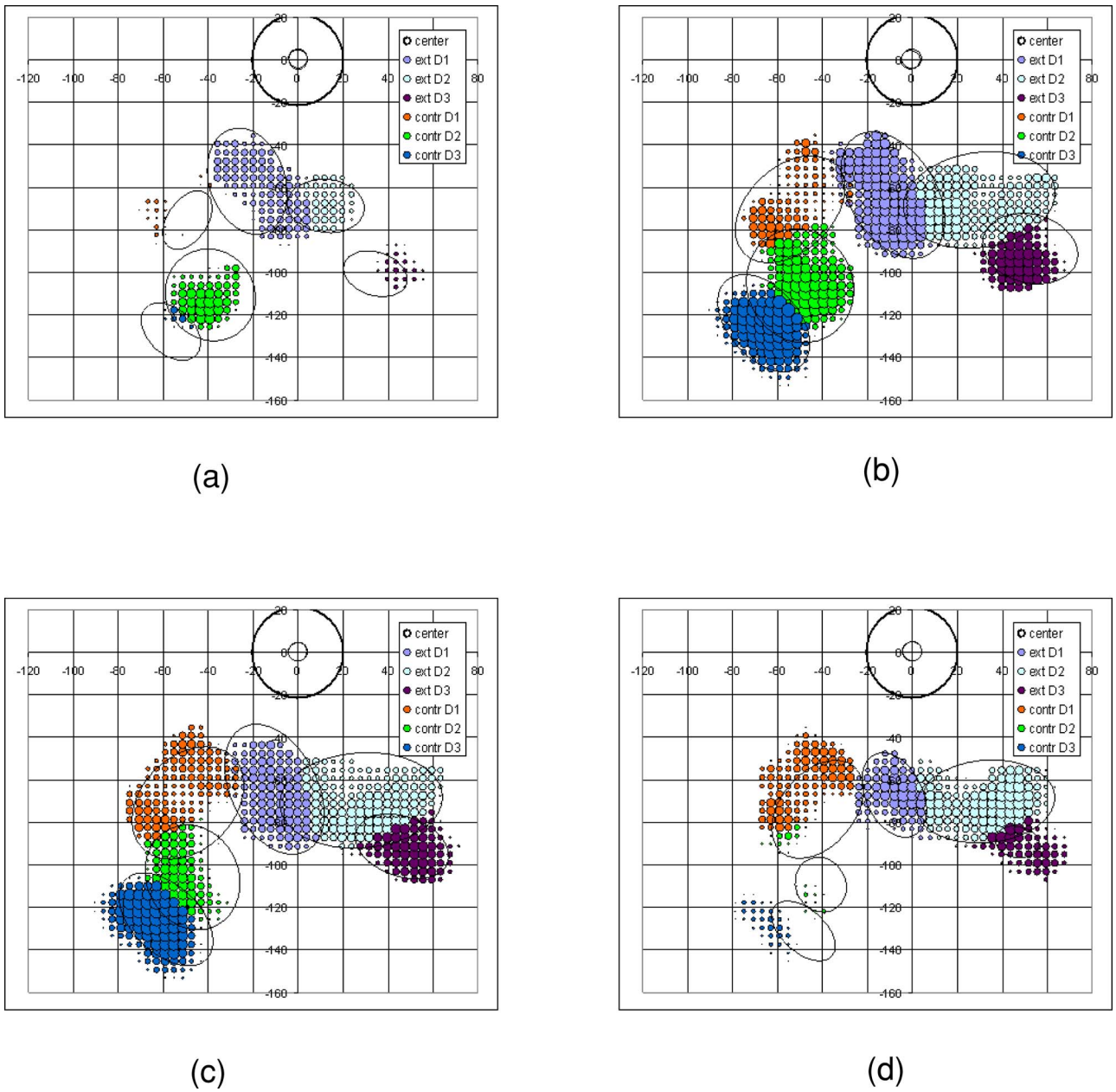

FIG. 15. (Color online) Comparison of electron density maps with ellipsoidal approximations, shown in cross sections along the Z axis (a) from -20 to -10 Å, (b) from -10 to 0 Å, (c) from 0 to 10 Å, and (d) from 10 to 20 Å. See text.

lattice parameters are likely to change a bit with "unrolling," leading to interfaces that differ somewhat from those shown in Fig. 13.

From Fig. 13 one can imagine the possibility of stress-inducing the transformation by shear as shown in Fig. 14. This would provide a direct measure of the relative heights of the energy wells and therefore of the contraction force. Ideally, one could begin with an epitaxially grown sheet, as discussed above, and release the film from the substrate on the medium gray region of Fig. 14; some of the techniques developed in the microactuator community [28] (such as backside etching) for patterning and releasing single crystal films could be relevant. Then by applying shear and slight extension as shown in Fig. 14 the phase transformation could be made to occur. Technically, the corners between phases may introduce stress concentrations in such an experiment, but this can be overcome by using a suitable indentor that induces an appropriate out-of-plane deformation. Once again, it would be fascinating to bring chemistry into such an experiment by altering the solution around the sheet.

ACKNOWLEDGMENTS

We thank Petr Leiman, Victor Kostyuchenko, and Michael Rossmann for the EM data and helpful discussions, and we wish to acknowledge helpful discussions with Gero Friesecke and John Maddocks. This work was supported by NSF-NIRT Grant No. DMS-0304326 and by the U.S. Army High Performance Computing Research Center under the auspices of the U.S. Department of the Army, Army Re-

search Laboratory cooperative agreement No. DAAD 191-01-2-0014.

APPENDIX: APPROXIMATION OF ELECTRON DENSITY MAPS

Many arguments of this paper relied on the approximate shape and orientation of the molecules. In order to have a reasonable but fairly simple representation of the molecules of the tail sheath, we approximated the electron density maps of Leiman *et al.* ([11]; we are grateful to Petr Leiman for providing prepublication data from high resolution cryoelectron micrographs of the extended sheath). Information about how the positions and orientations were extracted from the representations is given at the end of Sec. VI A.

The maps themselves showed clearly the presence of domains. These have the general appearance of nestled ellipsoids, so we approximated them by overlapping ellipsoids. We did this by partitioning the data by domain (the colored regions of Fig. 15). Then we computed the total electronic charge and center of mass of each domain. Using charge neutrality we made mass density proportional to electronic density. This can have errors arising mainly from the presence of H atoms, but in fact the total charge of a domain (or molecule) in the contracted vs the extended state differed by more than this error, so the quality of the data did not justify a more detailed analysis.

With the center of mass of the domain now fixed, we adjusted the principal axes of the ellipsoids to match approximately the sectional data. Sections of the selected ellipsoids are shown in Fig. 15 superimposed on the data. In this figure the concentric circles define the axis of the tail sheath and the Z values indicate the slices of the electron density map which were averaged. Here Z is an axial variable measured from a fixed (but arbitrary) reference. Domains for both extended and contracted sheath are shown. The ellipses are sections of the ellipsoid (for the enclosed domain) at the corresponding average value of Z (i.e., for $Z=0-10$ the slice through the ellipsoid was taken at $Z=5$).

[1] D. E. Smith, S. J. Tans, S. B. Smith, S. Grimes, D. L. Anderson, and C. Bustamante, Nature (London) **413**, 748 (2001).

[2] I. L. Ivanoska, P. J. de Pablo, B. Ibarra, G. Sgalari, F. C. MacKintosh, J. L. Carrascosa, C. F. Schmidt, and G. J. L. Wuite, Proc. Natl. Acad. Sci. U.S.A. **101**, 7600 (2004).

[3] J. F. Marko and E. D. Siggia, Macromolecules **28**, 8759 (1995).

[4] N. Chouaieb and J. H. Maddocks, J. Elast. **77**, 221 (2004).

[5] M. Moakher and J. H. Maddocks, Arch. Ration. Mech. Anal. **177**, 53 (2005).

[6] F. A. Eiserling, in *Bacteriophage T4*, edited by C. K. Mathews (American Society of Microbiology, Washington, D.C., 1983), pp. 11–24.

[7] G. B. Olson and H. Hartman, J. Phys. (Paris), Colloq. **43**, C4-855 (1982).

[8] H. R. Crane, Sci. Mon. **70**, 376 (1950).

[9] J. L. Ericksen, in *Advances in Applied Mechanics*, edited by C.-S. Yih (Academic Press, New York, 1977), Vol. 17, pp. 189–244.

[10] M. G. Rossmann, V. V. Mesyanzhinov, F. Arisaka, and P. G. Leiman, Curr. Opin. Struct. Biol. **14**, 171 (2004).

[11] P. G. Leiman, P. R. Chipman, V. A. Kostyuchenko, V. V. Mesyanzhinov, and M. G. Rossmann, Cell **118**, 419 (2004).

[12] V. A. Kostyuchenko, P. R. Chipman, P. G. Leiman, F. Arisaka, V. V. Mesyanzhinov, and M. G. Rossmann, Nat. Struct. Mol. Biol. **12**, 810 (2005).

[13] L. Pauling, Discuss. Faraday Soc. **13**, 170 (1953).

[14] P. G. de Gennes, *The Physics of Liquid Crystals* (Oxford University Press, Oxford, 1974).

[15] M. F. Moody, J. Mol. Biol. **80**, 618 (1973).

[16] R. D. James and K. F. Hane, Acta Mater. **48**, 197 (2000).

[17] F. Arisaka, J. Engel, and H. Klump, Prog. Clin. Biol. Res. **64**, 365 (1981).

[18] P. K. Purohit, J. Kondev, and R. Phillips, Proc. Natl. Acad. Sci. U.S.A. **100**, 3173 (2003).

[19] M. Arroyo and T. Belytschko, J. Mech. Phys. Solids **50**, 1941 (2002).

[20] G. Friesecke, R. D. James, and S. Müller, Arch. Ration. Mech. Anal. (to be published).

[21] J. P. Sethna, Phys. Rev. B **31**, 6278 (1985).

[22] N. R. M. Watts and D. H. Coombs, J. Virol. **64**, 143 (1990).

[23] P. Krulevitch, A. P. Lee, P. B. Ramsey, J. C. Trevino, J. Hamilton, and M. A. Northrup, J. Microelectromech. Syst. **5**, 270 (1996).

[24] K. Bhattacharya and R. D. James, Science **307**, 53 (2005).

[25] E. Kellenberger and E. Boy De La Tour, J. Ultrastruct. Res. **11**, 545 (1964).

[26] C. M. To, E. Kellenberger, and A. Eisenstark, J. Mol. Biol. **46**, 493 (1969).

[27] S. Lee, C. Mao, C. E. Flynn, and A. M. Belcher, Science **296**, 892 (2002).

[28] J. W. Dong, J. Q. Xie, J. Lu, C. Adelmann, C. J. Palmstrom, J. Cui, Q. Pan, R. D. James, and S. McKernan, J. Appl. Phys. **95**, 2593 (2004).

[29] K. Bhattacharya and R. D. James, J. Mech. Phys. Solids **46**, 531 (1999).